Electronic Supplementary Material (ESI) for Nanoscale.

Supplementary information for

Controllable Synthesis of Hollow Mesoporous Organosilica Nanoparticles with Pyridine-2,6-Bis-Imidazolium Frameworks for CO_2 Conversion

Ghazale Anvarian-Asl,[a] Sadegh Joudian,[a] Stefano Todisco,[b] Pietro Mastrorilli,[b] and Mojtaba Khorasani*[a,c]

[a] Department of Chemistry, Institute for Advanced Studies in Basic Sciences (IASBS), No. 444, Prof. Yousef Sobouti Boulevard, Zanjan 45137-66731, Iran. E-mail: m_khorasani@iasbs.ac.ir, Fax: +98-24-33153232; Tel: +98-24-3315-3223.

b Dipartimento di Farmacia-Scienze del Farmaco, Università degli Studi di Bari, Aldo Moro, Via Edoardo Orabona 4, Bari I-70125, Italy

[c] Research Center for Basic Sciences & Modern Technologies (RBST), Institute for Advanced Studies in Basic Sciences, IASBS, Zanjan 45137-66731, Iran.

Table of Contents

1. Materials and methods

1.1. Characterization

The particle morphology of the prepared materials was monitored by transmission electron microscopy (Philips CM120) as well as scanning electron microscope (SEM, TESCAN MIRA3 FE-SEM). For SEM, the samples were deposited on a sample holder with an adhesive carbon foil and sputtered with gold. Elemental mapping results were obtained by an energy dispersive spectrometer (EDS) attached to the SEM apparatus. Using standard continuous procedures, N_2 adsorption isotherms were measured at 77 K by Belsorp (BELMAX, Japan) analyzer where samples were first pretreated at 353 K for 5 h. The specific surface area was determined from the linear part of the BET plot ($P/P_0 \approx 0.05$-0.15), the pore size distribution was calculated using the Barrett–Joyner–Halenda (BJH) method from the adsorption branch of nitrogen isotherm, and the total pore volume was estimated based on the total N_2 adsorbed at $P/P_0 \approx 0.995$. Powder X-ray diffraction patterns were carried out using a PANalytical (XPert PRo MPD) with CuK_α ($\lambda = 1.518$ Å), a minimum step size of 0.0001°. Thermogravimetric analysis was performed by using a NETZSCH STA 409 PC/PG instrument at scan rates of 20 K min^{-1}, with typically a 5 mg sample under flowing N_2. Solid State NMR experiments were performed on a Bruker Avance I 400 spectrometer (^{13}C, 100.6 MHz; ^{29}Si 79.5 MHz) using a 4.0 mm HX MAS probe at 298 K. FT-IR spectra were recorded on a Brüker EQUINOX-55 instrument equipped with a liquid N_2-cooled MCT detector. X-ray photoelectron spectroscopy, XPS [BESTEC (EA 10)] determined the oxidation state of surface elements in the catalyst. Gas chromatography analyses were performed on Varian CP-3800 using a flame ionization detector (FID) using trimethylbenzene (TMB) as suitable internal standards. NMR spectra were recorded using a Brüker (^1H frequency: 400 MHz, ^{13}C frequency: 100 MHz).

1.2. Synthesis

1.2.1. Synthesis of Cu-HMON-L-C-2.5

A mixture of Cl-HMON-L-C-2.5 (0.2 g) and CuI (0.023 g) in DMSO (3 mL), under an inert atmosphere of Ar, was heated from RT to 160 ºC and then held at 160 ºC for ca. 5 h. The mixture was then allowed to cool to RT. The solid was collected, washed with ethanol (60 mL), and then air-dried. Loading of Cu was found to be 0.12 mmol $g^{-}1$ by using Inductively coupled plasma mass spectrometry (ICP-MS).[S1]

1.2.2. Synthesis of 2,6-(bis-methyl imidazolium)pyridine chloride:

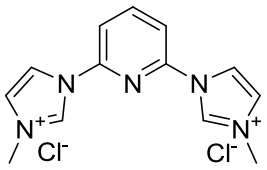

2,6-chloropyridine (0.76 g, 5.13 mmol) was mixed with 1-methylimidazole (1.69 g, 20.6 mmol) in a double-necked glass balloon under an argon atmosphere. The reaction mixture was allowed to stir at 145 °C for 72 h affording a light brown solid. The solid was washed several times with dichloromethane and tetrahydrofuran (THF) to obtain white powder.[S2]

1.2.3. Synthesis of 2,6-(bis-N-methyl imidazolium)pyridine iodide:

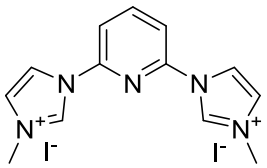

The homemade 2,6-(bis-methyl imidazolium)pyridine chloride (0.2 g) was added to a 50 ml glass balloon containing 25 ml dichloromethane (DCM) and allowed to sonicate for 15 minutes. Then tetrabutylammonium iodide (1.6 g) in 2 ml of DCM was added

and the mixture was stirred for 5h. Then, the solid was separated from the suspension carefully washed with DCM and acetone and dried under a vacuum overnight.

1.2.4. Synthesis of 1-benzyl-4-phenyl-1H-1,2,3-triazole:

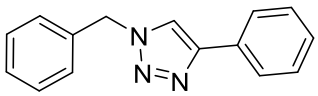

Phenylacethylene (0.3 mmol), benzyl azide (0.3 mmol) and Cu-HMON-L-C-2.5 (0.007 g) were added to DI-water (3ml). The reaction mixture was stirred for 5 h at 70 °C. After cooling the mixture to room temperature, the aqueous phase was extracted by ethyl acetate. Then, the organic layer was removed by reduced pressure to obtain pure corresponding 1,2,3-triazole product.

1.2.5. Synthesis of I-MON

at first, Cl-MON was synthesized as follows. In a round bottom flask, 600 mg of CTAB was dissolved in 300 ml distilled water and 168 mg NaOH. At 80 °C, the mixture was stirred for 30 minutes to dissolve the surfactant completely. To the surfactant solution, 13.43 mmol of pre-synthesized pyridine-2,6-bis-imidazolium organosilica precursor (0.2 g, 0.33 mmol) and TEOS (2.65 g, 13.4 mmol) were gently added dropwise with stirring in a 2.5:97.5 ratio. Immediately, a white suspension was formed, which was then stirred at 80 °C for two hours. After centrifuging, the powder was washed twice with water and ethanol. As-synthesized Cl-MON was mixed with 100 ml of an ethanolic solution of ammonium nitrate at 65 °C for 8 hours to remove the CTAB template. This process was repeated twice. Then, the resulted Cl-MON (0.5 g) was added to DI-water (15 ml) and allow to sonicated for at least 10 minutes and followed by addition of a saturated solution of KI in DI-water. The mentioned suspension was stirred for 8 h at room temperature. The resulting catalyst denoted

as I-MON was then washed severally with DI-water and acetone and finally dried under vacuum at 60 °C overnight.

2. References

[S1] D. H. Brown and B. W. Skelton, *Dalton Trans*., 2011, *40*, 8849-8858.

[S2] D. Domyati, S. L. Hope, R. Latifi, M. D. Hearns, and L. Tahsini, *Inorg. Chem*., 2016, *55*, 11685-11693.

3. Tables

Table S1. Textural properties of the synthesized mesoporous organosilicas were determined from nitrogen physisorption data.

Entry	Materials	S_{BET}	V_t	D_p
1	Cl-HMON-L-A-1	333	0.4	3.3
2	Cl-HMON-L-A-2.5	369	0.69	5.4
3	Cl-HMON-L-A-5	296	0.49	4.2
4	Cl-HMON-L-B-1	667	0.87	2.4
5	Cl-HMON-L-B-2.5	630	1.18	2.4
6	Cl-HMON-L-C-1	953	1.4	2.4
7	Cl-HMON-L-C-2.5	738	1.38	2.4
8	Cl-HMON-S-D-2.5	227	0.23	2.4
9	Cl-HMON-S-D-5	84	0.45	2.4
10	I-MON	513	1.34	2.4

[a] S_{BET}: Specific surface area was determined from the linear part of the BET plot ($P/P_0 \approx 0.05$-0.15). [b] V_t: Total pore volume based on the N_2 adsorbed at $P/P_0 \approx 0.995$. [c] D_{BJH}: Pore size distribution calculated from the adsorption branch using BJH methods.

Table S2: Reusability results for I-HMON-L-C-2.5.[a]

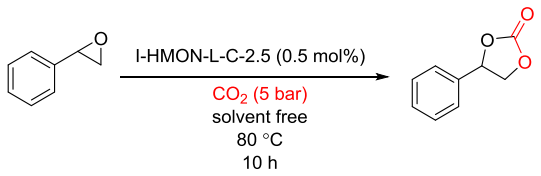

Run	Yield (%)[b]	TON[c]
1	94	188
2	93	186
3	92	184
4	92	184
5	93	186
6	93	186

[a]Reaction conditions: Styrene oxide (5 mmol), I-HMON-L-C-2.5 (0.5 mol%, 0.043 g), CO_2 (5 bar) at 80 °C.
[b] GC yield by using TMB as an internal standard.
[c] TONs were determined by (mmol of styrene carbonate)/(mmol of iodide).

5. Scheme

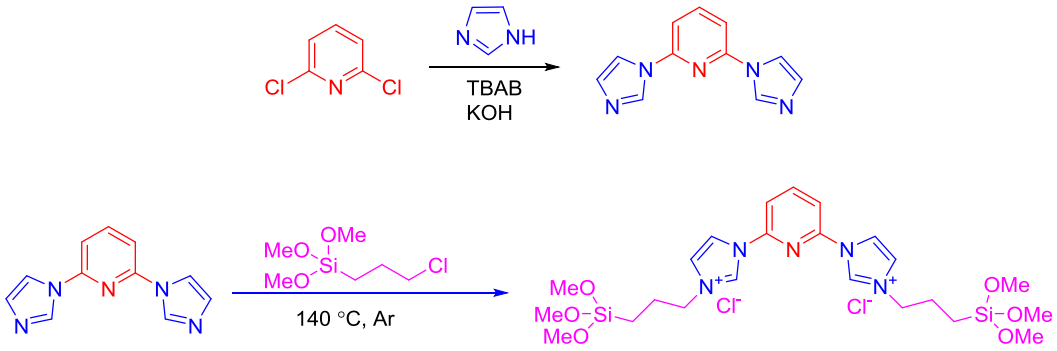

Scheme S1. Schematically representation for synthesis method of organosilica precursor preparation

6. Figures

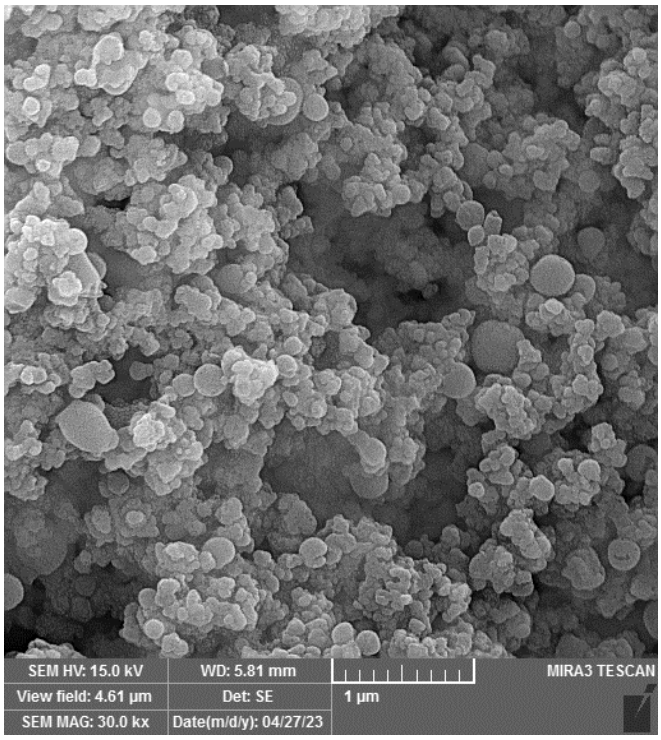

Figure S1. SEM image for as-synthesized Cl-HMON-L-B-2.5

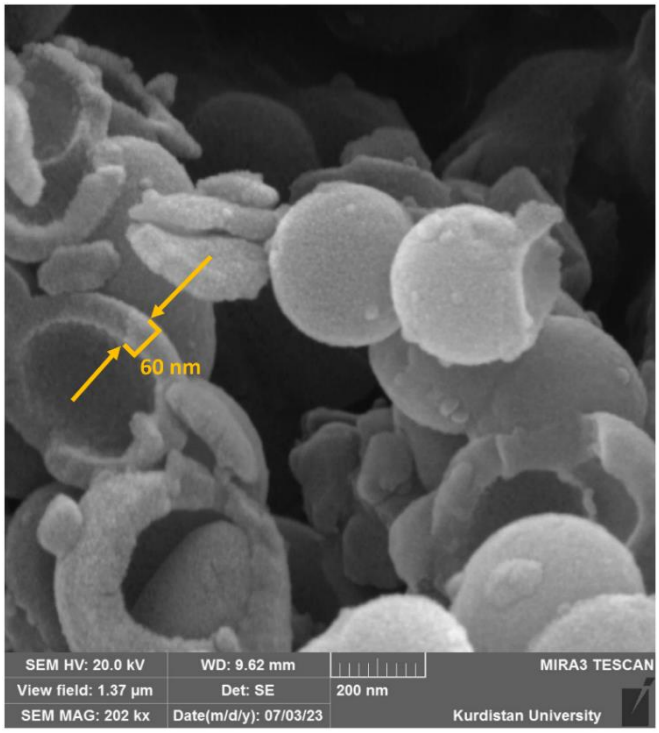

Figure S2. SEM image for Cl-HMON-L-B-1

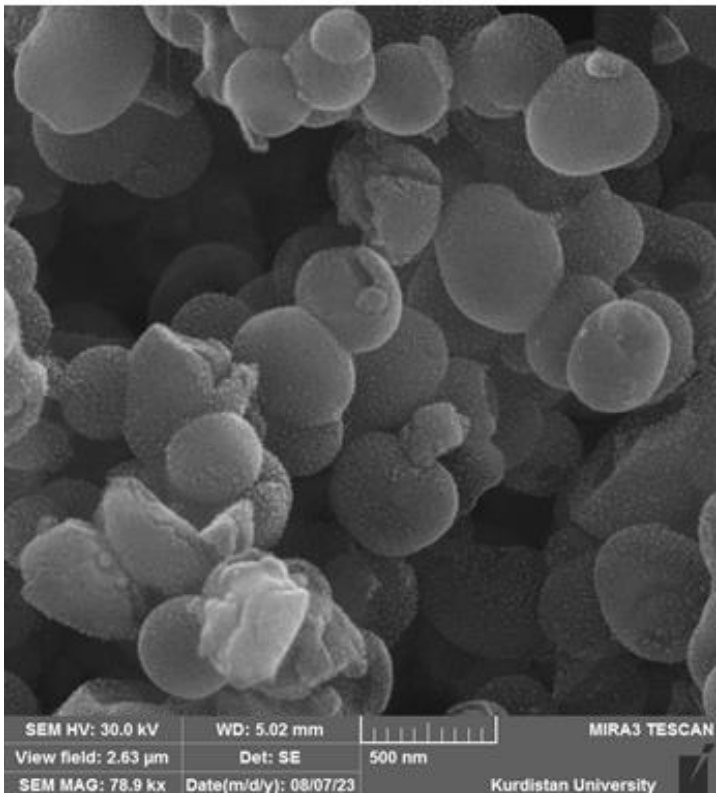

Figure S3. SEM image of I-HMON-L-B-1

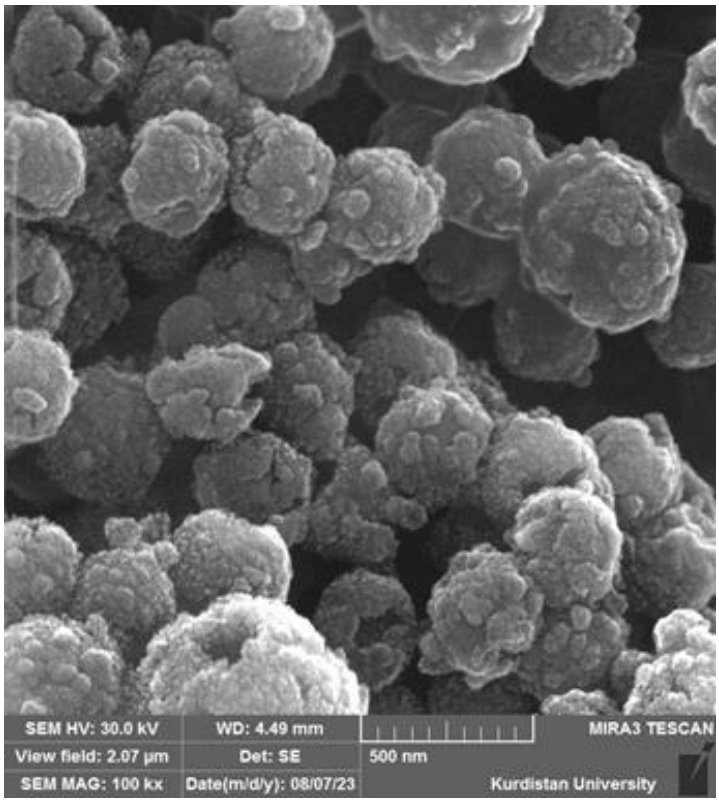

Figure S4. SEM image of I-HMON-L-C-1

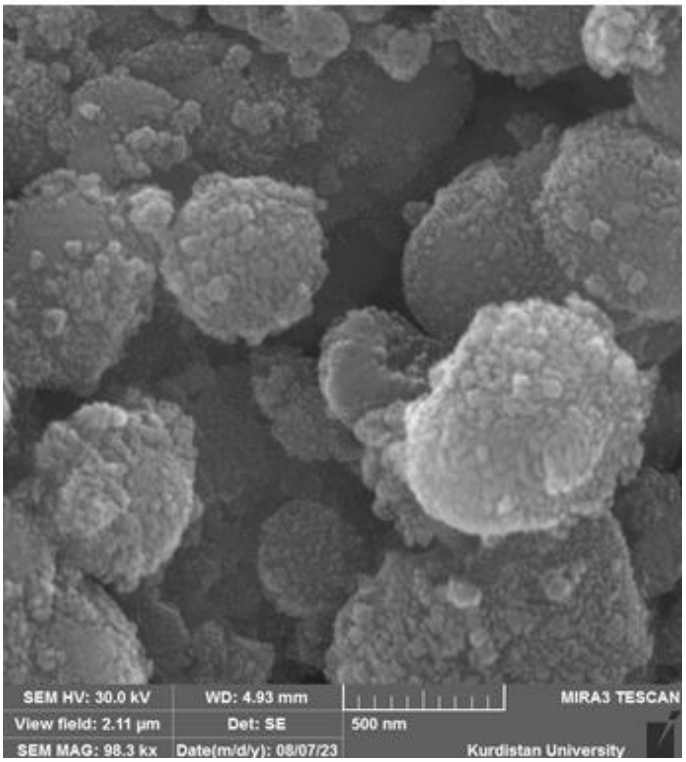

Figure S5. SEM image of I-HMON-L-C-2.5

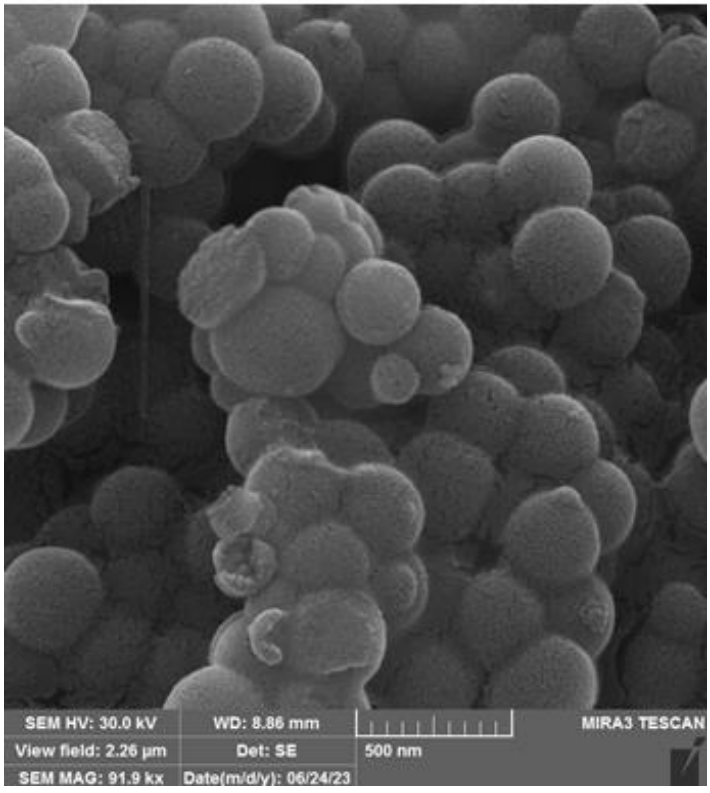

Figure S6. SEM image of I-HMON-S-D-2.5

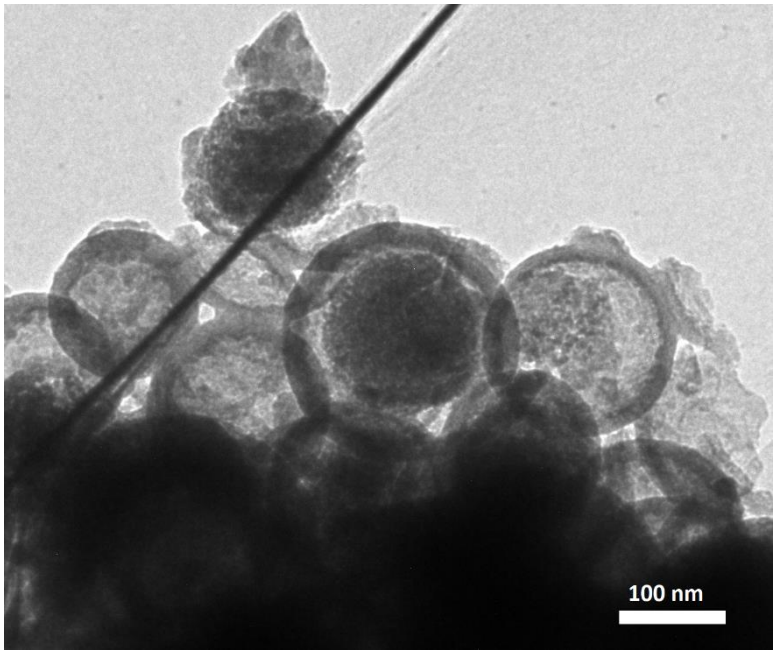

Figure S7. TEM image for Cl-HMON-L-B-1

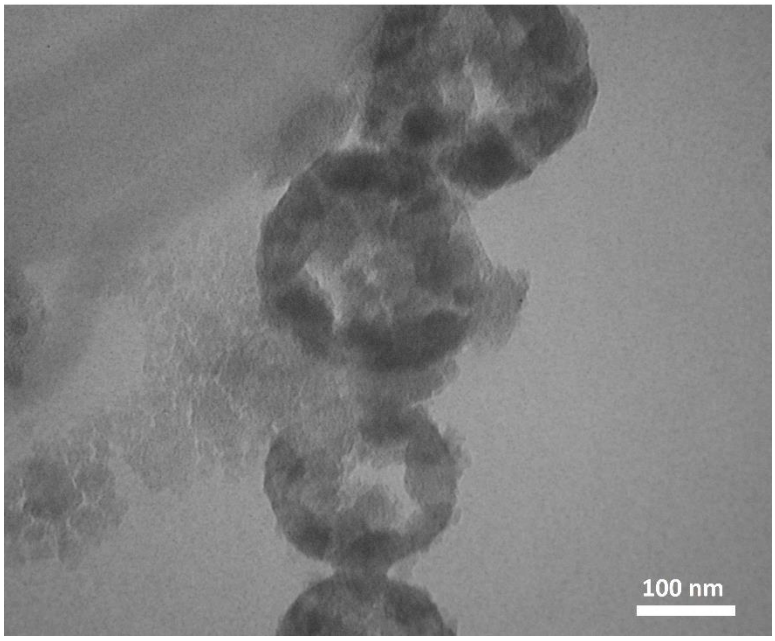

Figure S8. TEM image for Cl-HMON-L-C-1

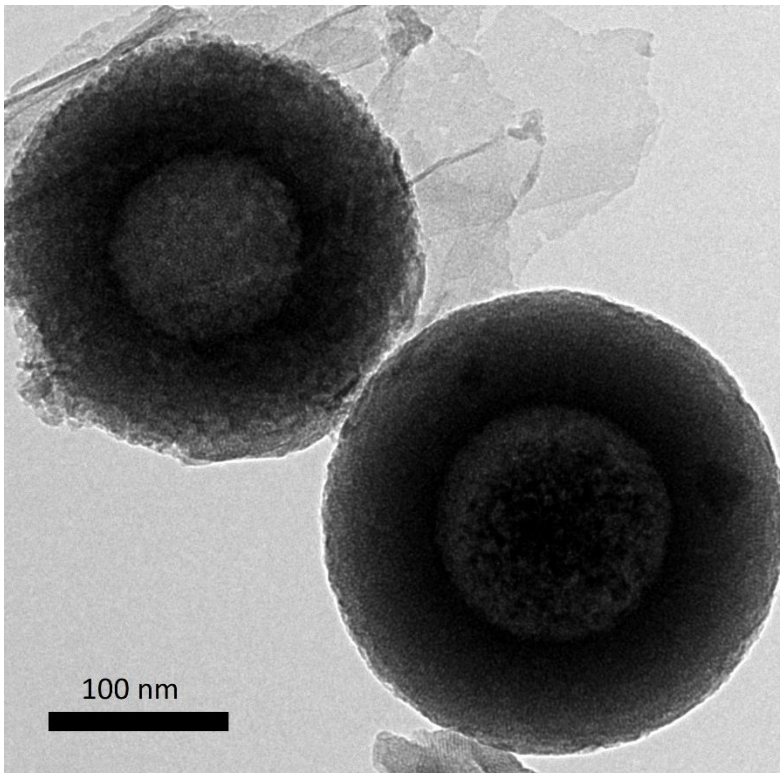

Figure S9. TEM image for Cl-HMON-L-C-2.5

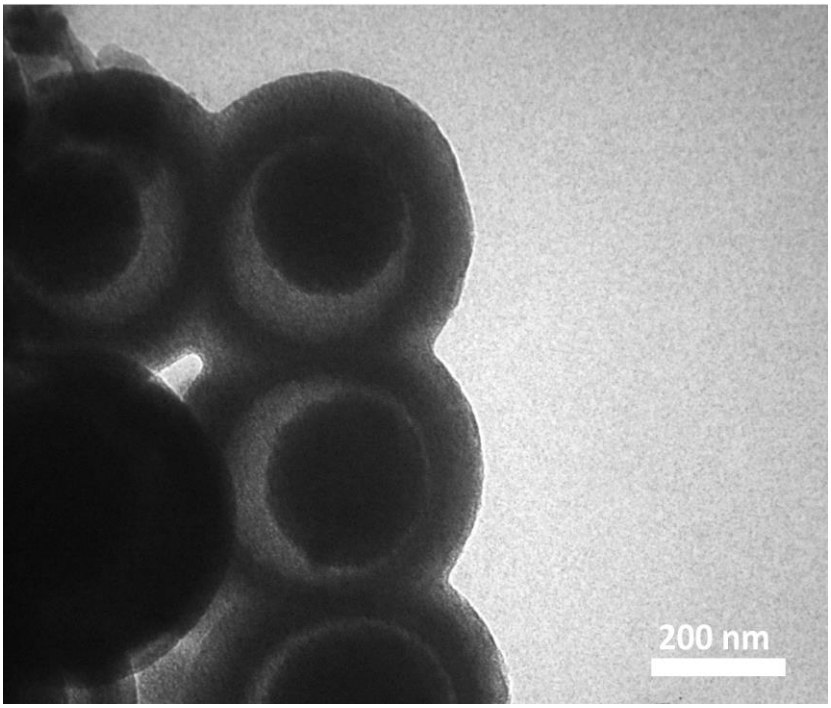

Figure S10. TEM image for Cl-HMON-S-D-2.5

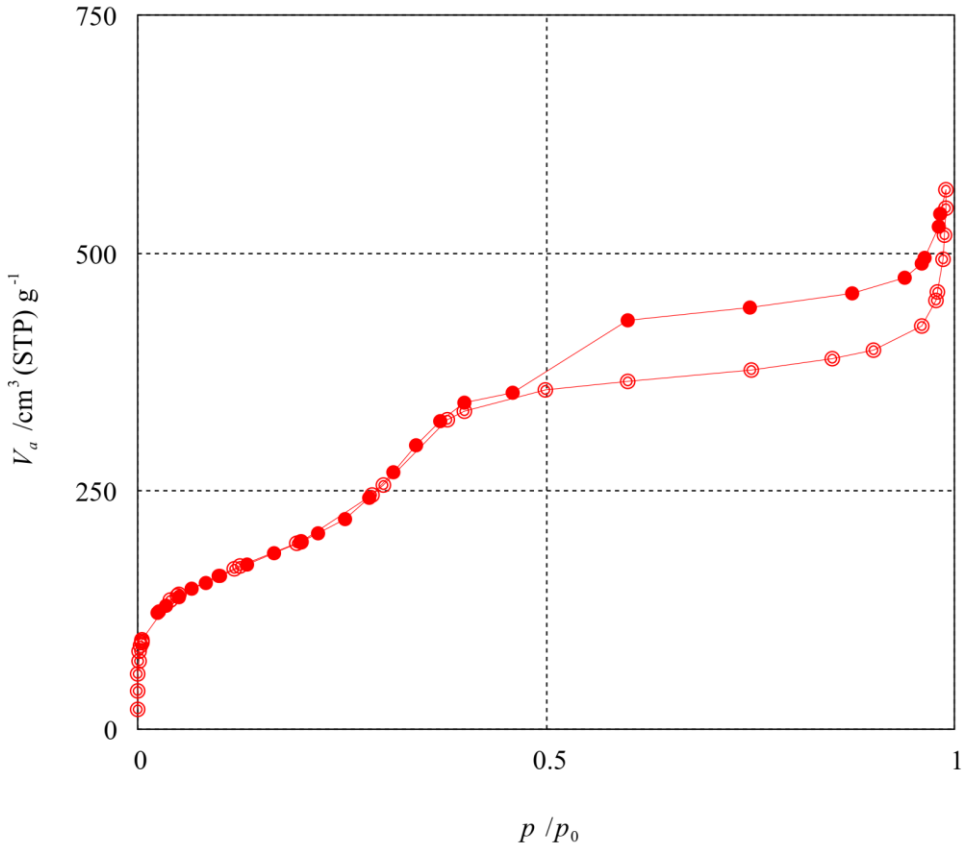

Figure S11. Nitrogen adsorption-desorption isotherm for Cl-HMON-L-B-1

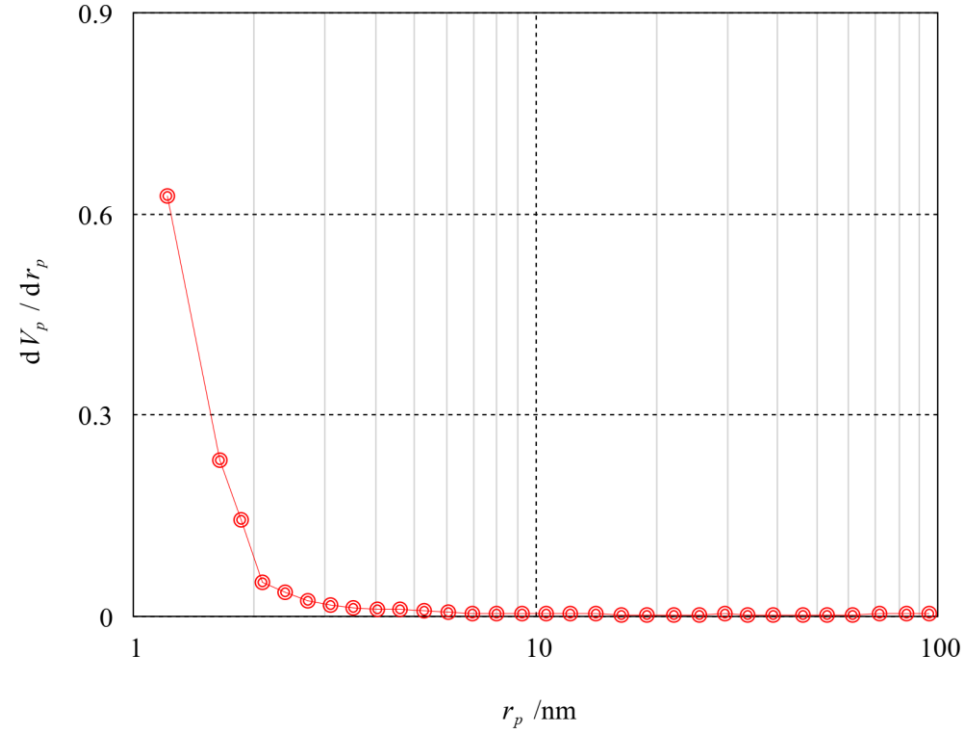

Figure S12. BJH pore side distribution for Cl-HMON-L-B-1

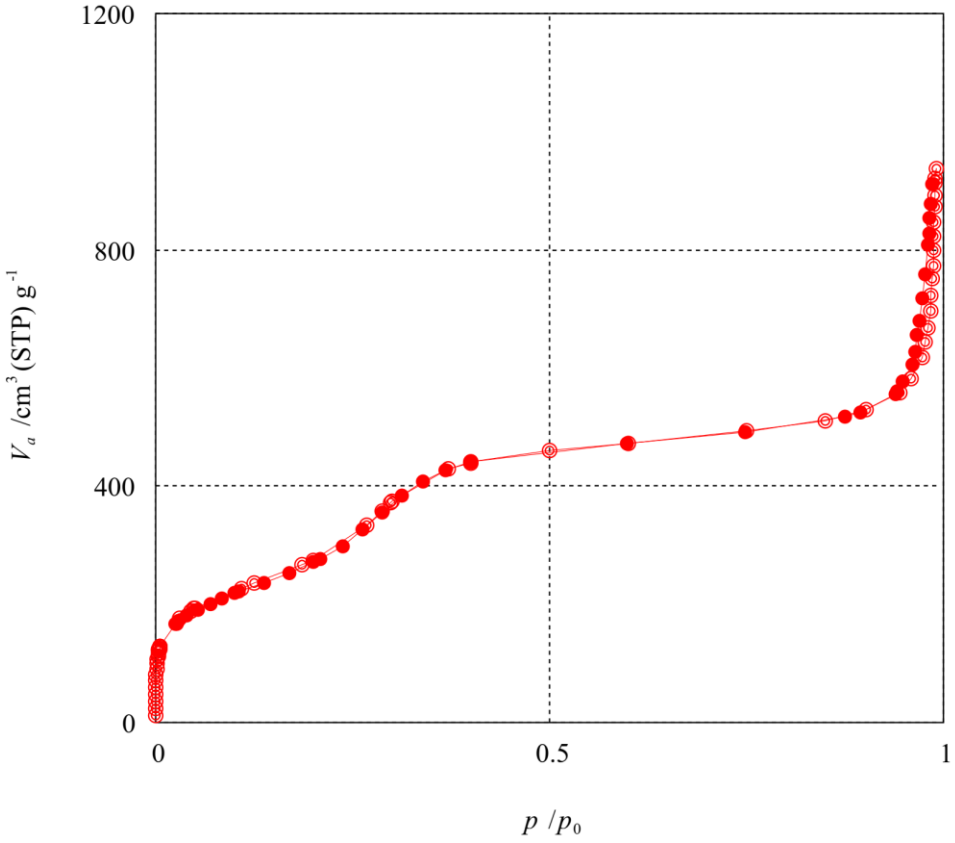

Figure S13. Nitrogen adsorption-desorption isotherm for Cl-HMON-L-C-1

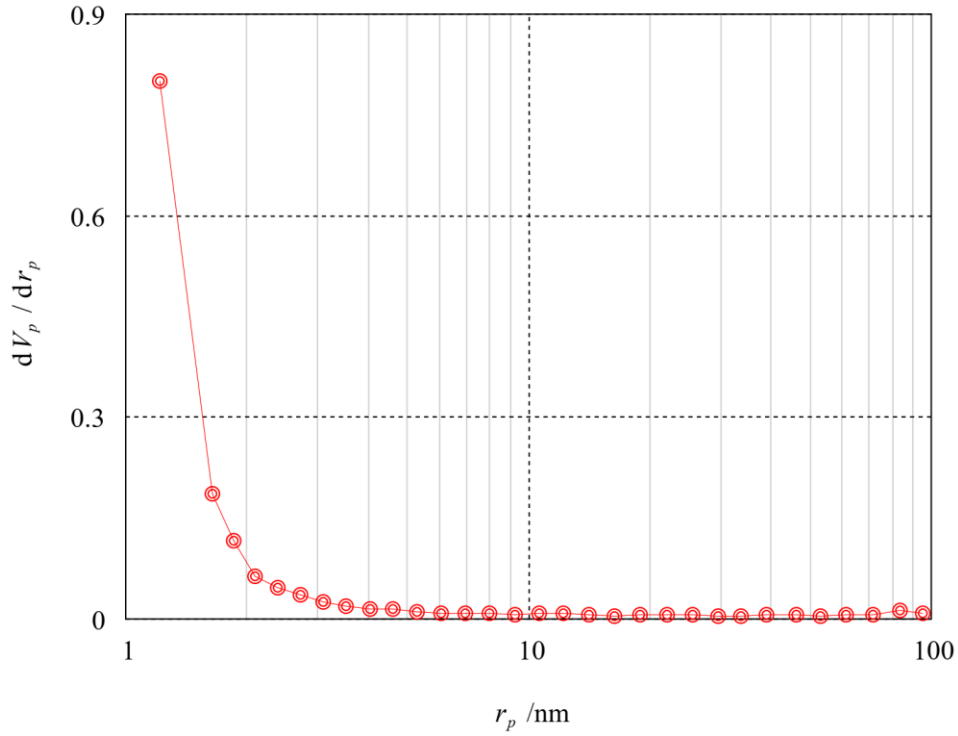

Figure S14. BJH pore size distribution for Cl-HMON-L-C-1

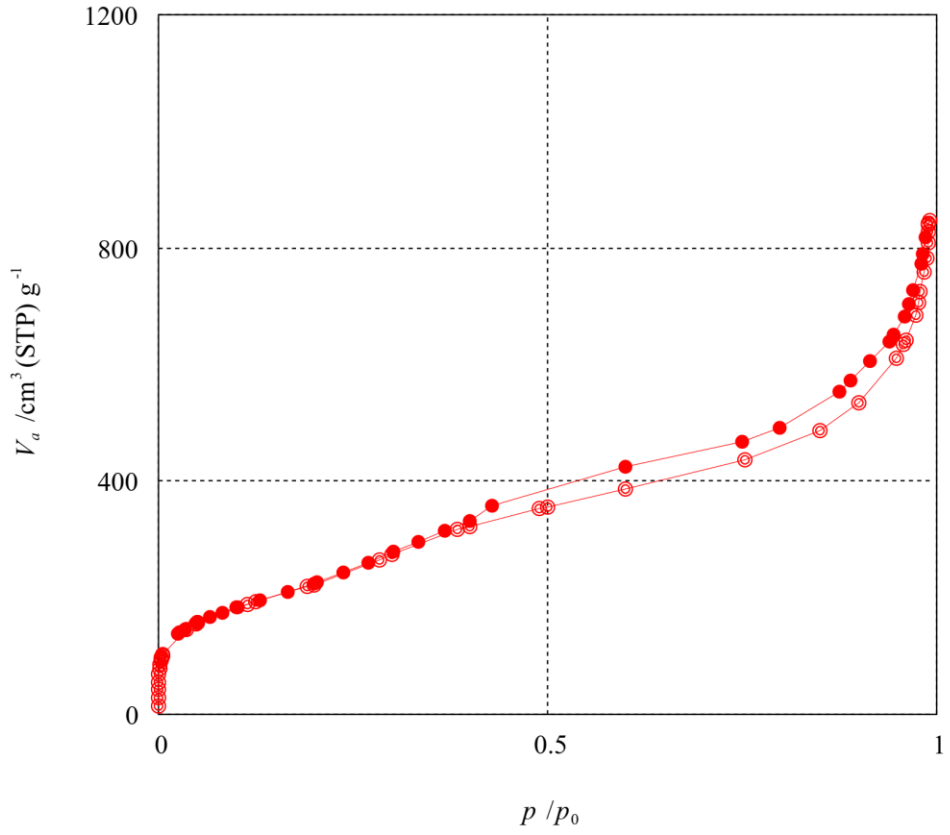

Figure S15. Nitrogen adsorption-desorption isotherm for Cl-HMON-L-C-2.5

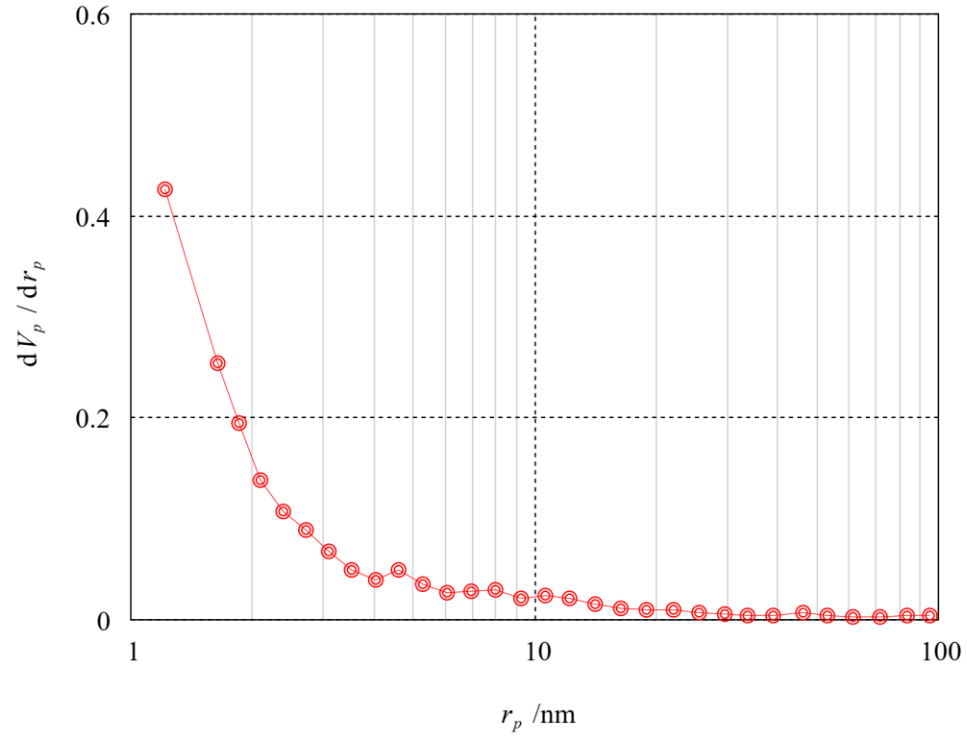

Figure S16. BJH pore size distribution for Cl-HMON-L-C-2.5

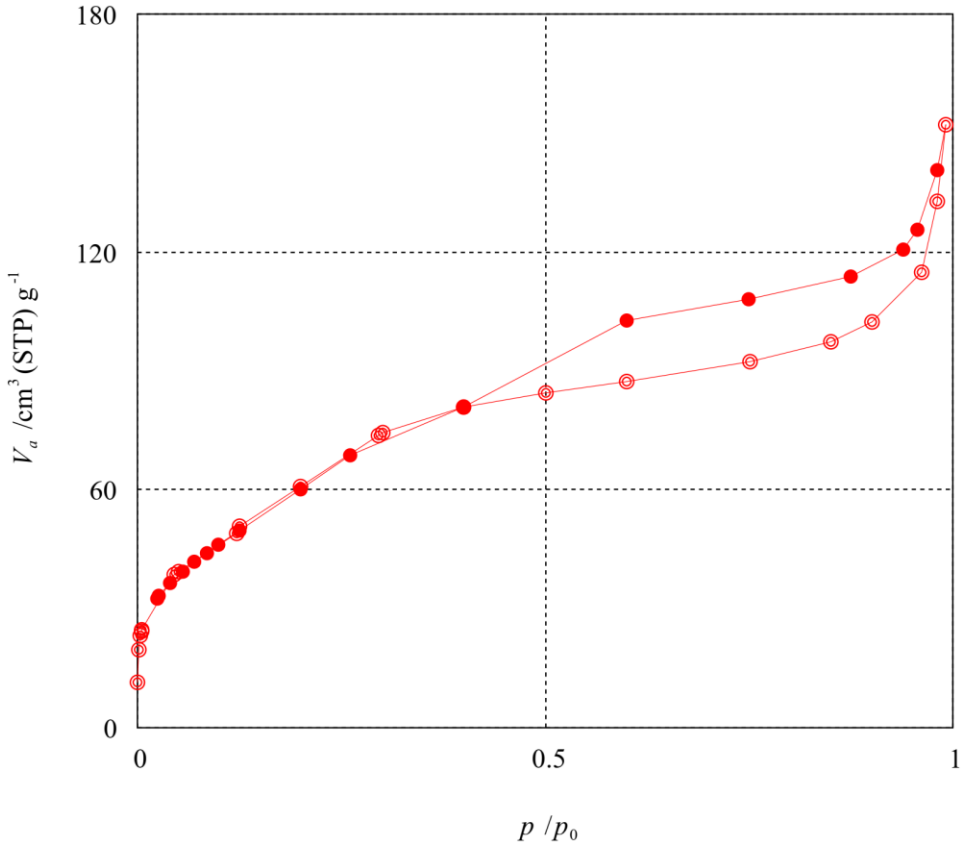

Figure S17. Nitrogen adsorption-desorption isotherm for Cl-HMON-S-D-2.5

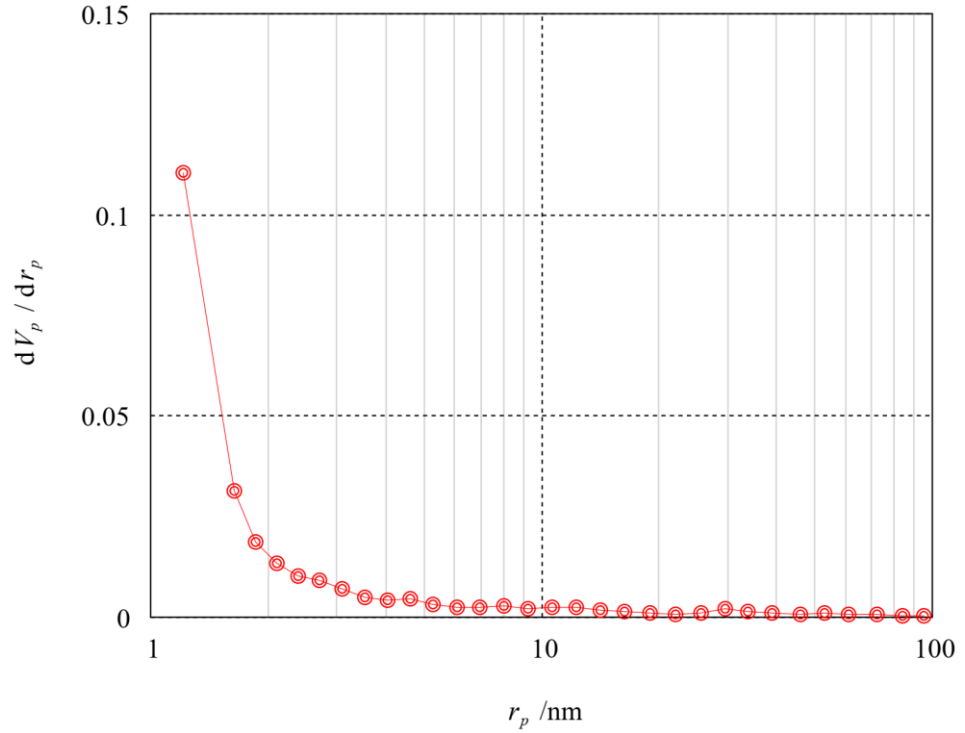

Figure S18. BJH pore size distribution for Cl-HMON- S-D-2.5

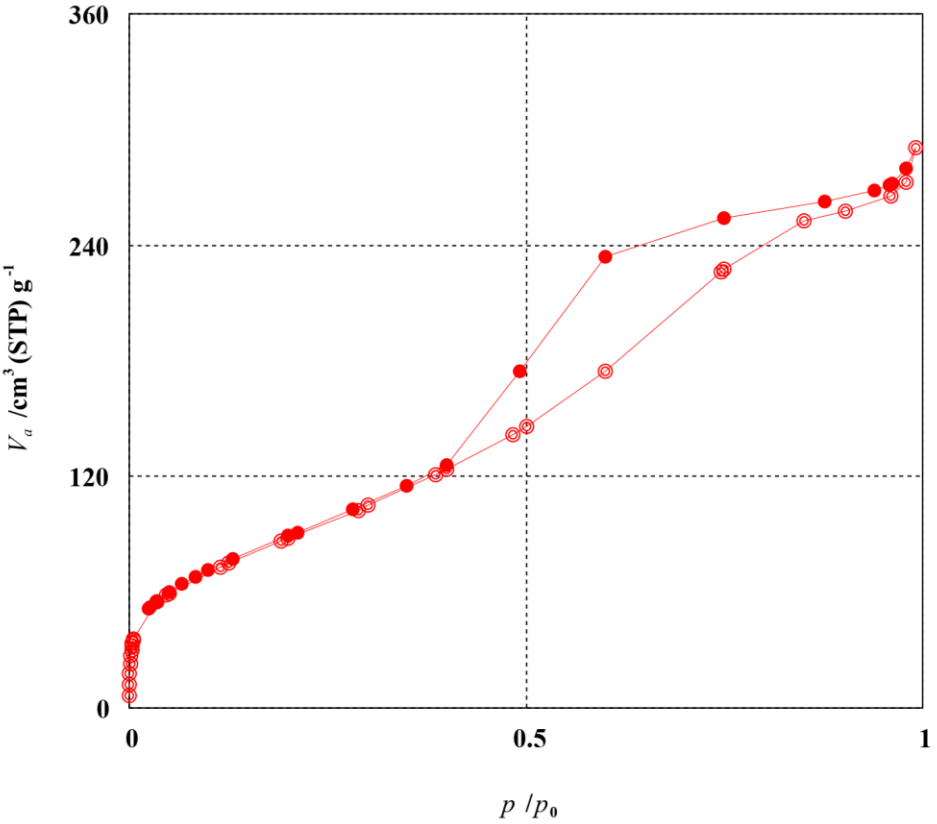

Figure S19. Nitrogen adsorption-desorption isotherm for Cl-HMON-A-1

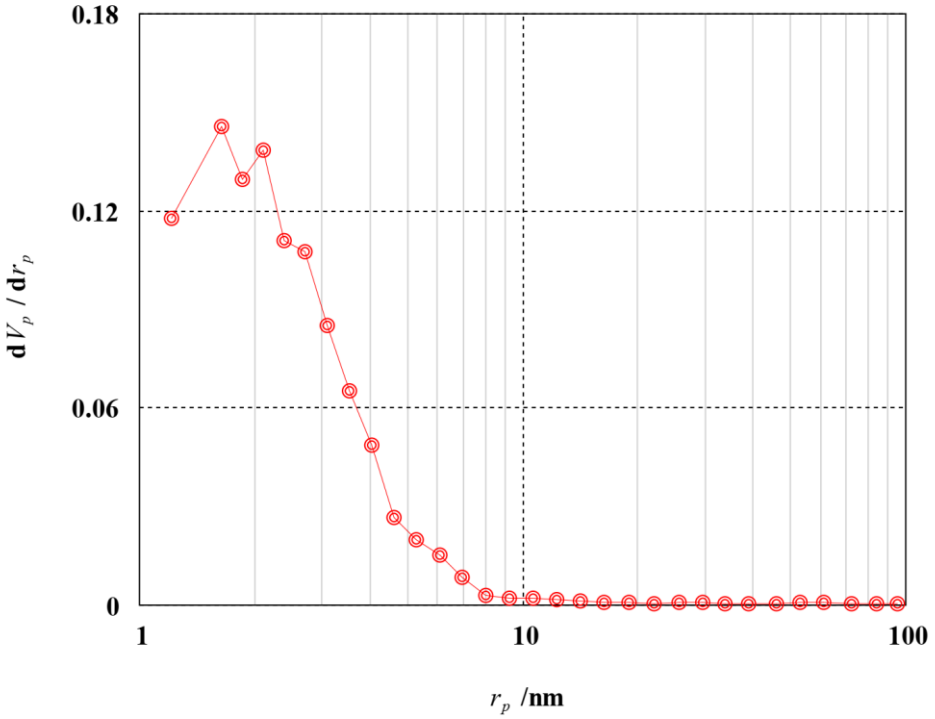

Figure S20. BJH pore size distribution for Cl-HMON-A-1

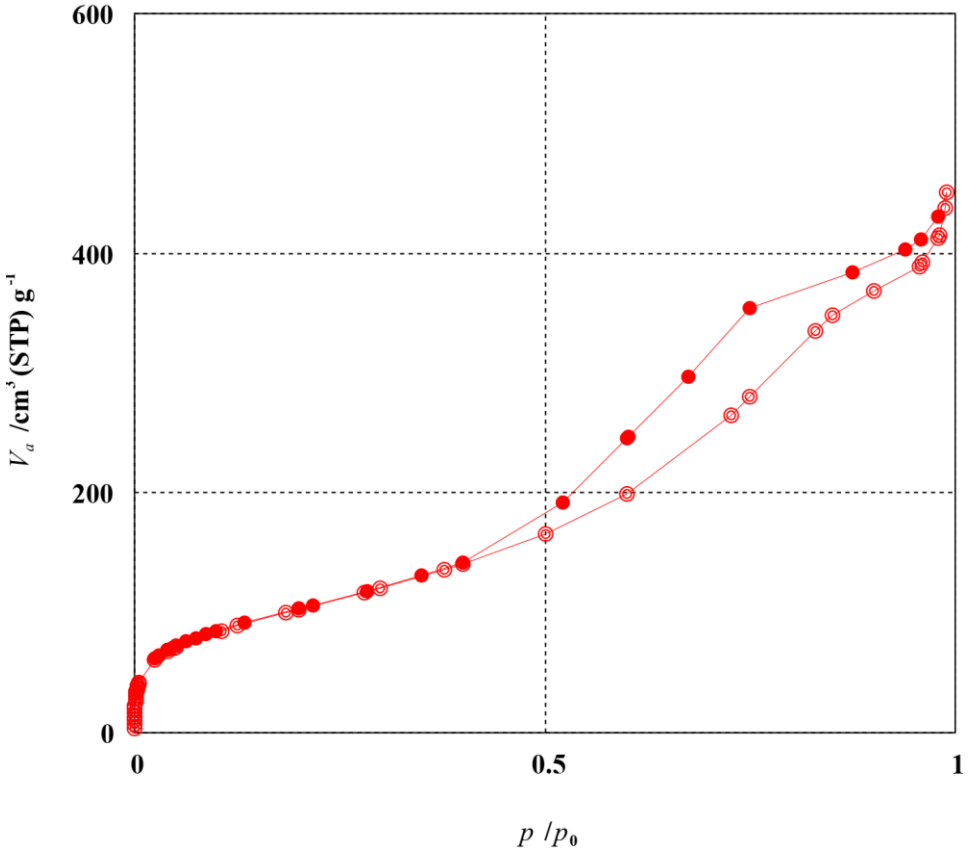

Figure S21. Nitrogen adsorption-desorption isotherm for Cl-HMON-L-A-2.5

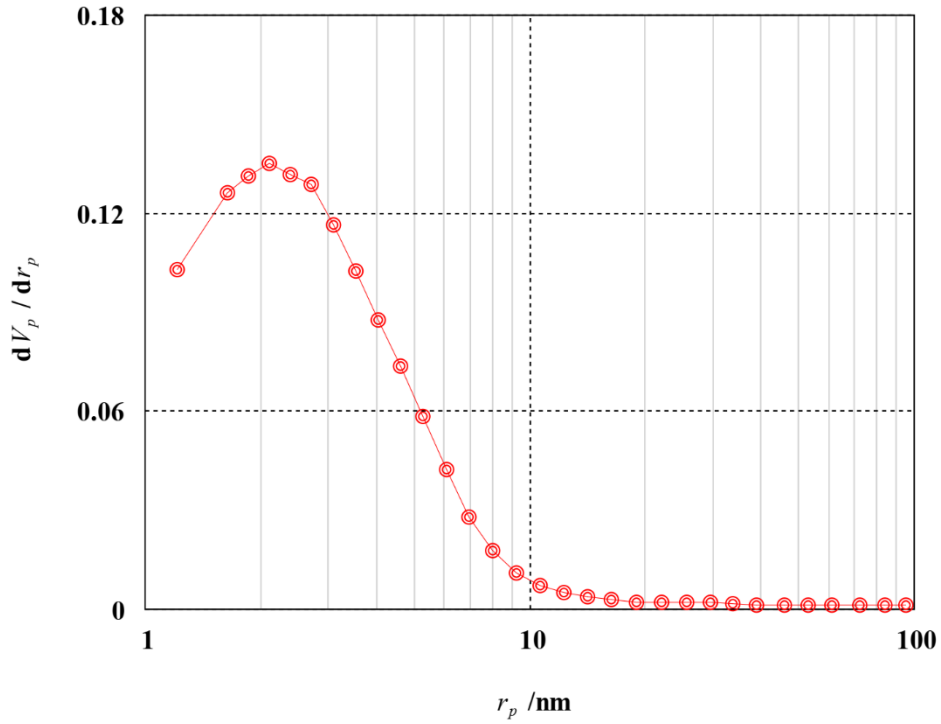

Figure S22. BJH pore size distribution for Cl-HMON-L-A-2.5

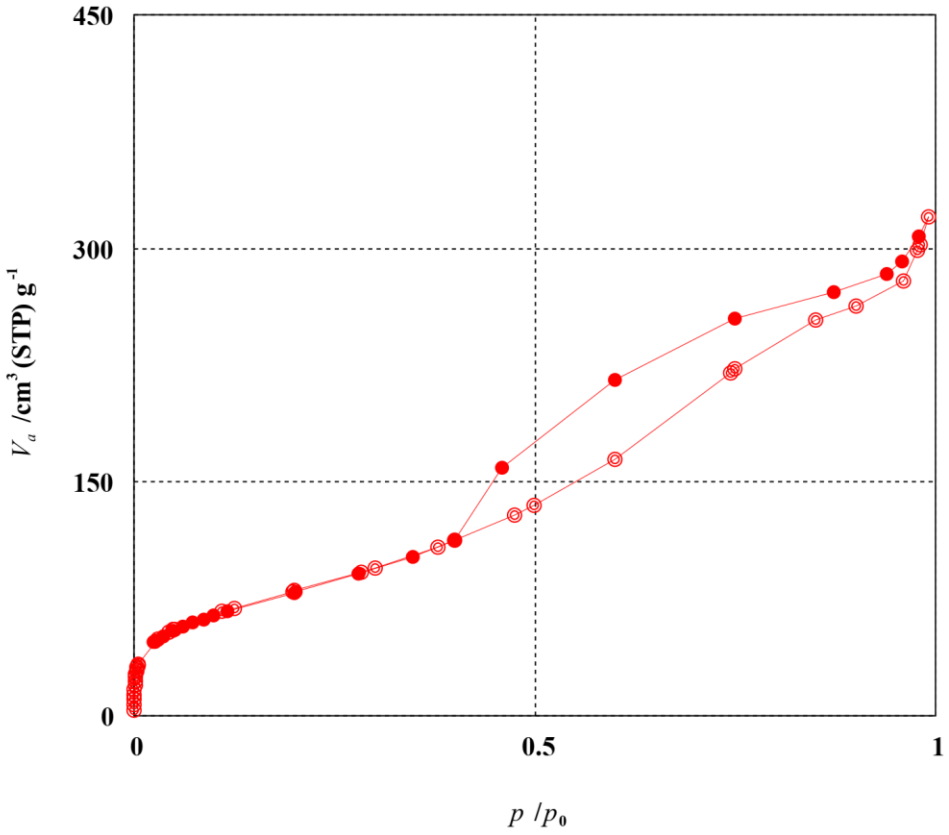

Figure S23. Nitrogen adsorption-desorption isotherm for Cl-HMON-L-A-5

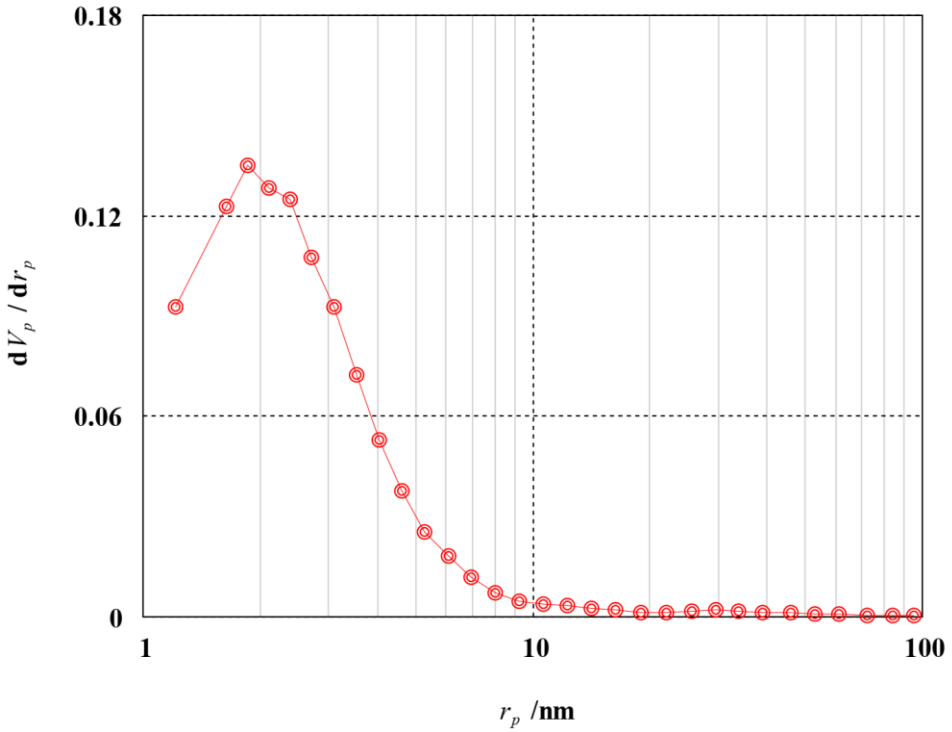

Figure S24. BJH pore size distribution for Cl-HMON-L-A-5

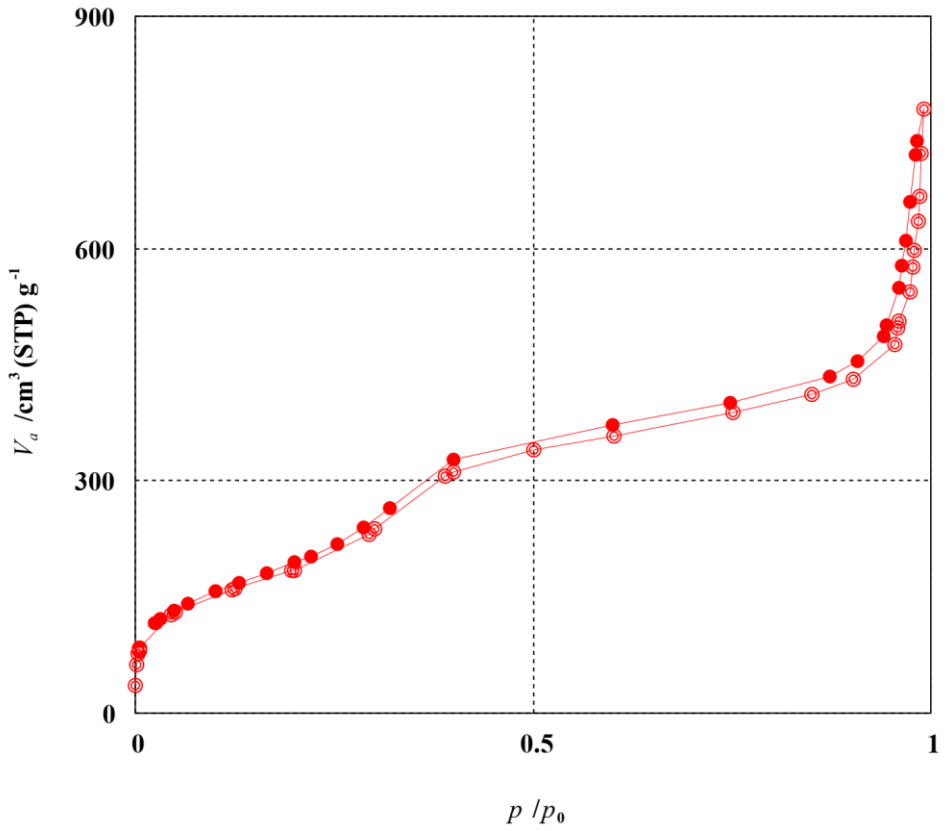

Figure S25. Nitrogen adsorption-desorption isotherm for Cl-HMON-L-B-2.5

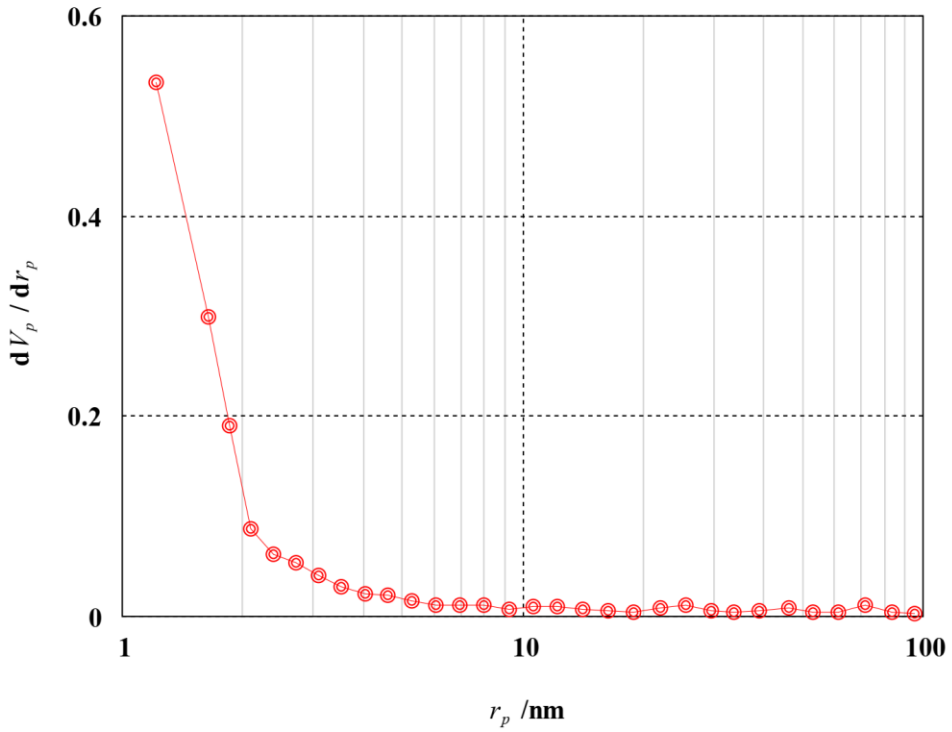

Figure S26. BJH pore size distribution for Cl-HMON-L-B-2.5

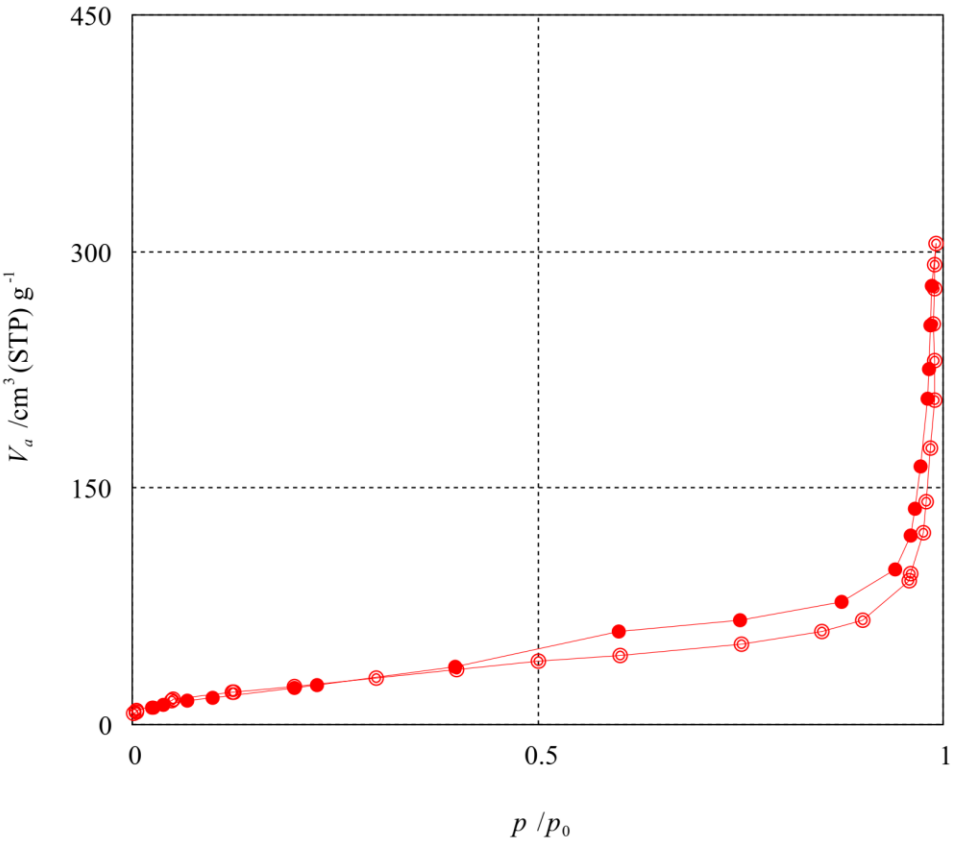

Figure S27. Nitrogen adsorption-desorption isotherm for Cl-HMON-S-D-5

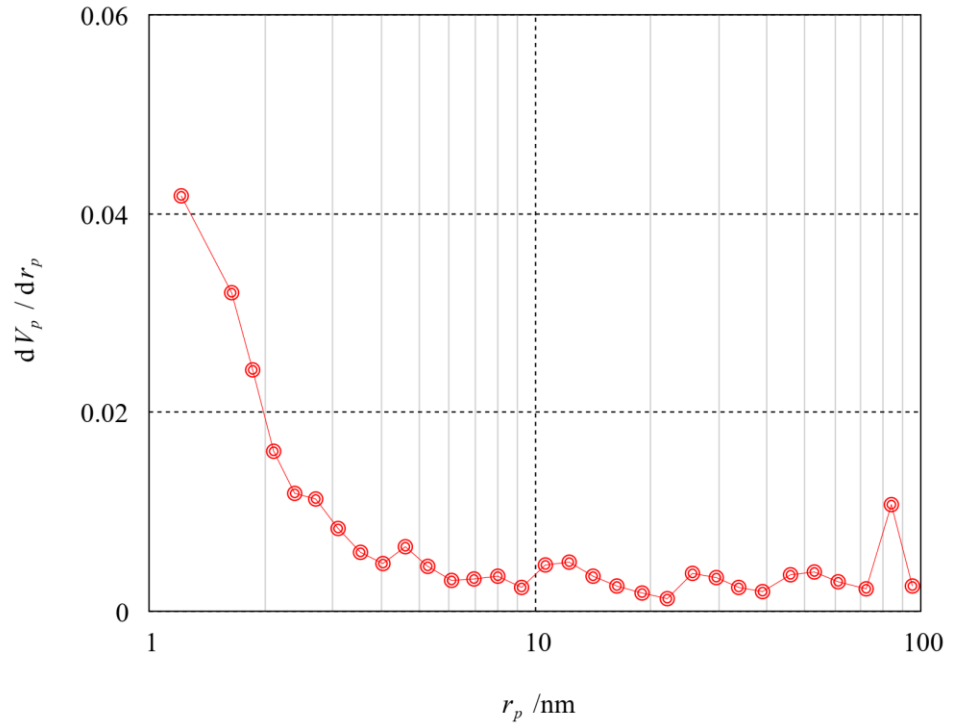

Figure S28. BJH Cl-HMON-S-D-5

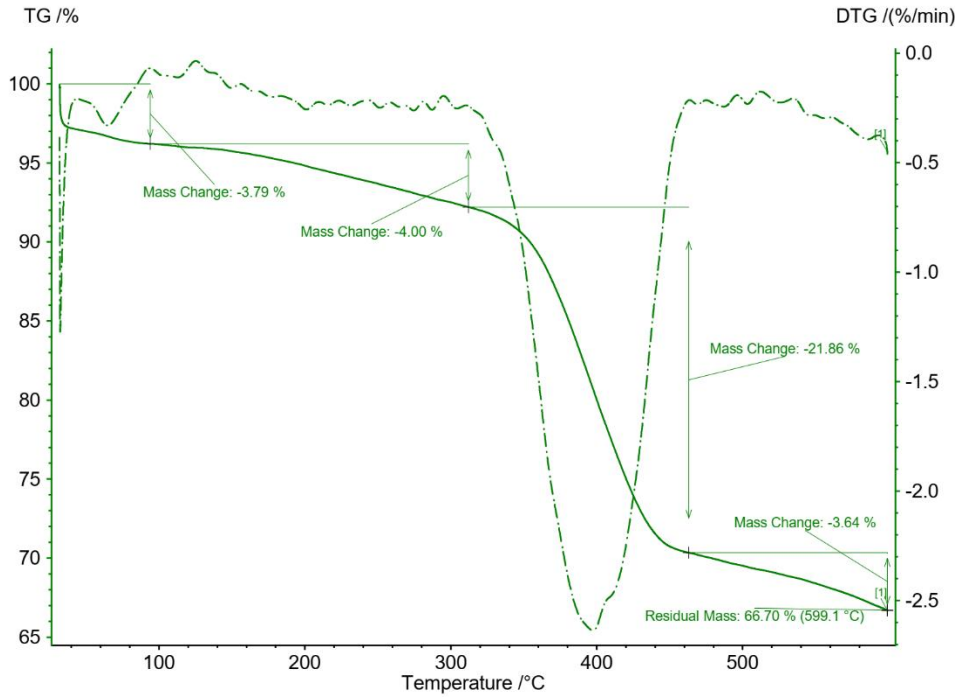

Figure S29. TGA patterns for I-HMON-L-B-1

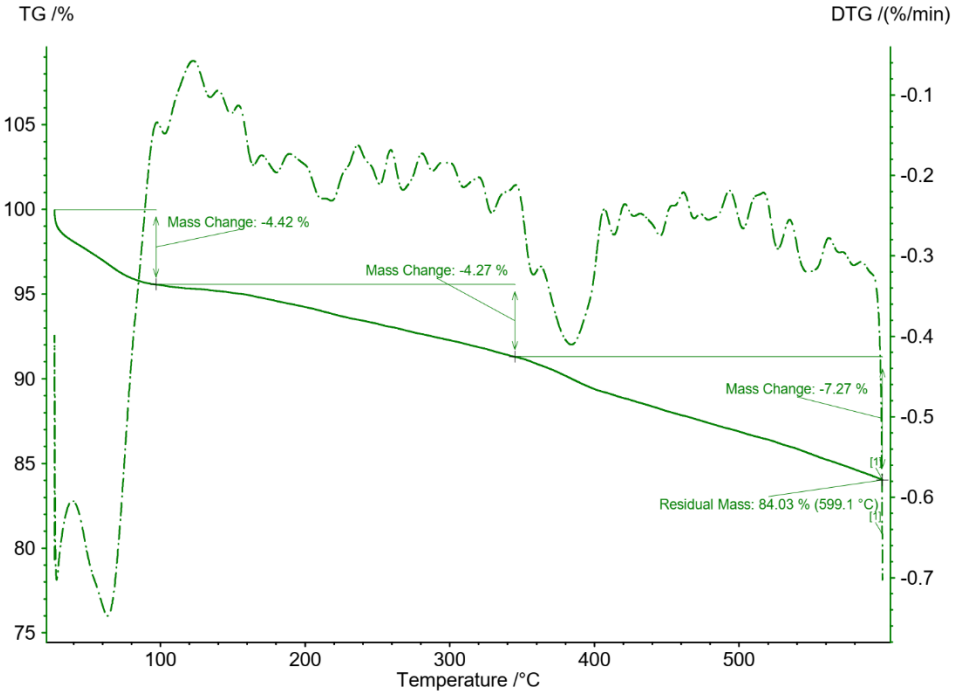

Figure S30. TGA patterns for I-HMON-L-C-1

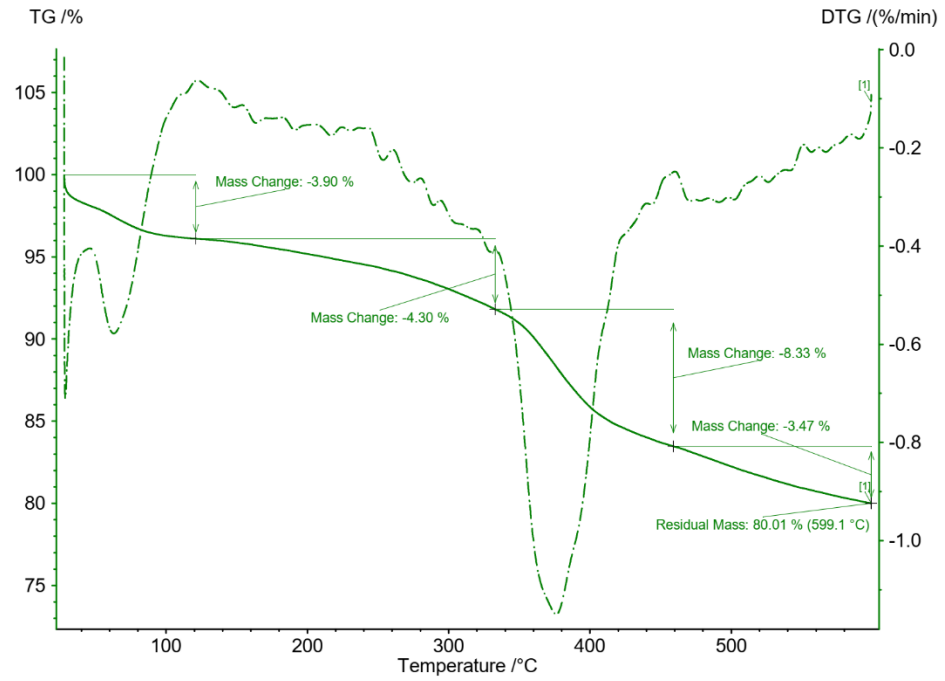

Figure S31. TGA patterns for I-HMON-L-C-2.5

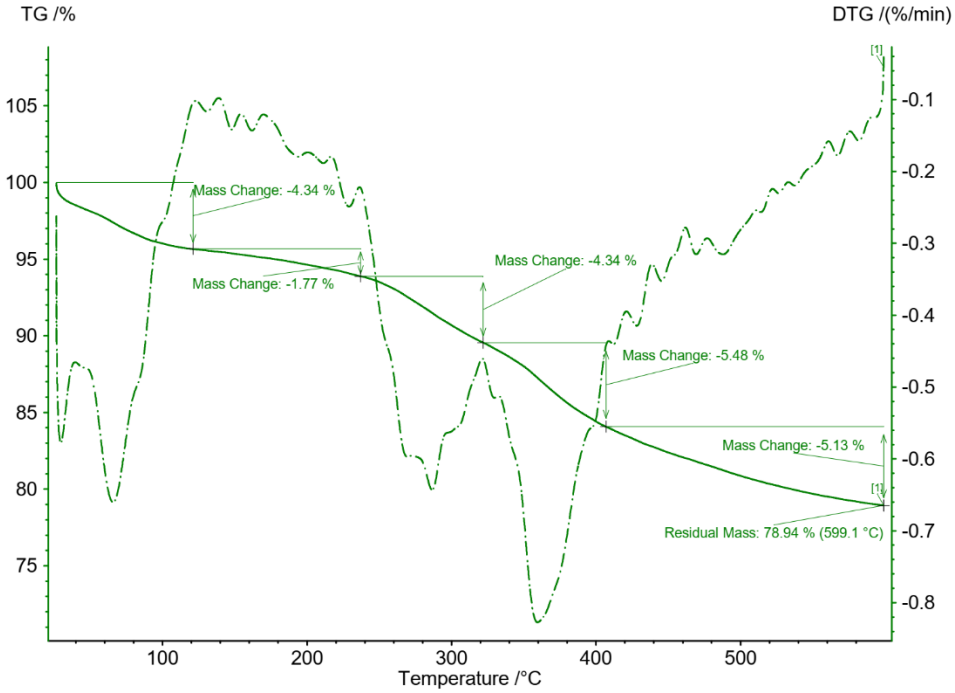

Figure S32. TGA patterns for I-HMON-S-D-2.5

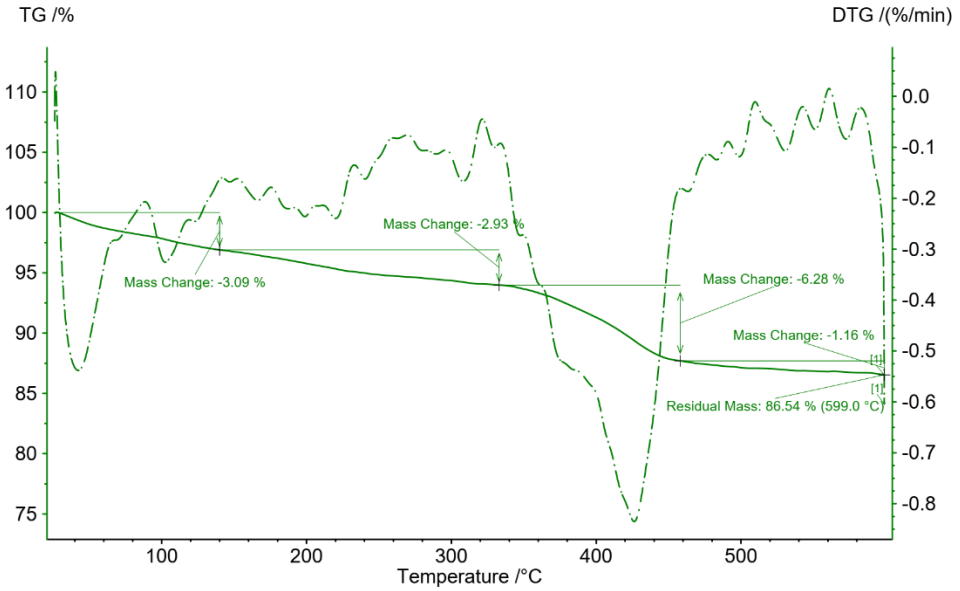

Figure S33. TGA patterns for Cl-HMON-L-A-1

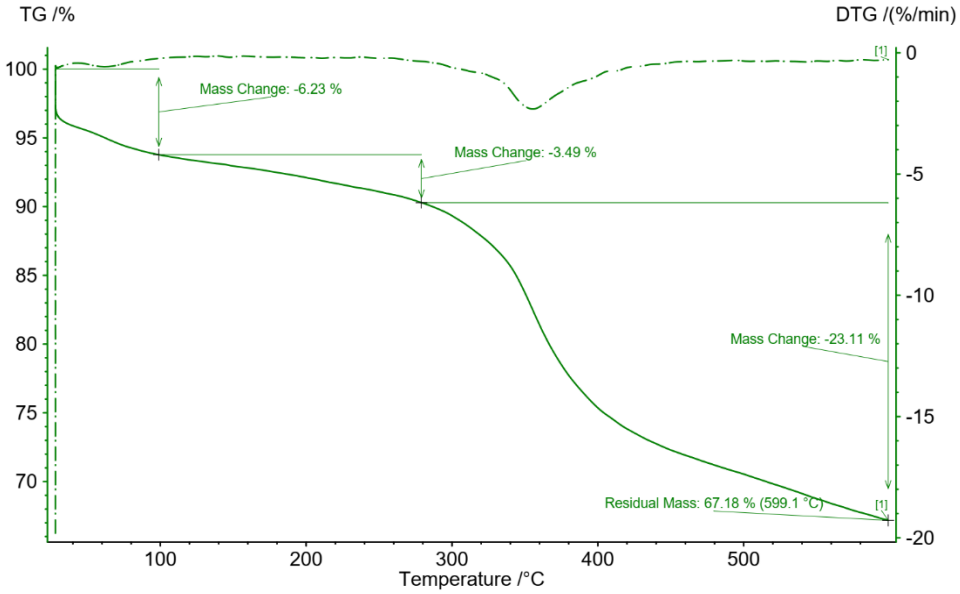

Figure S34. TGA patterns for Cl-HMON-L-A-2.5

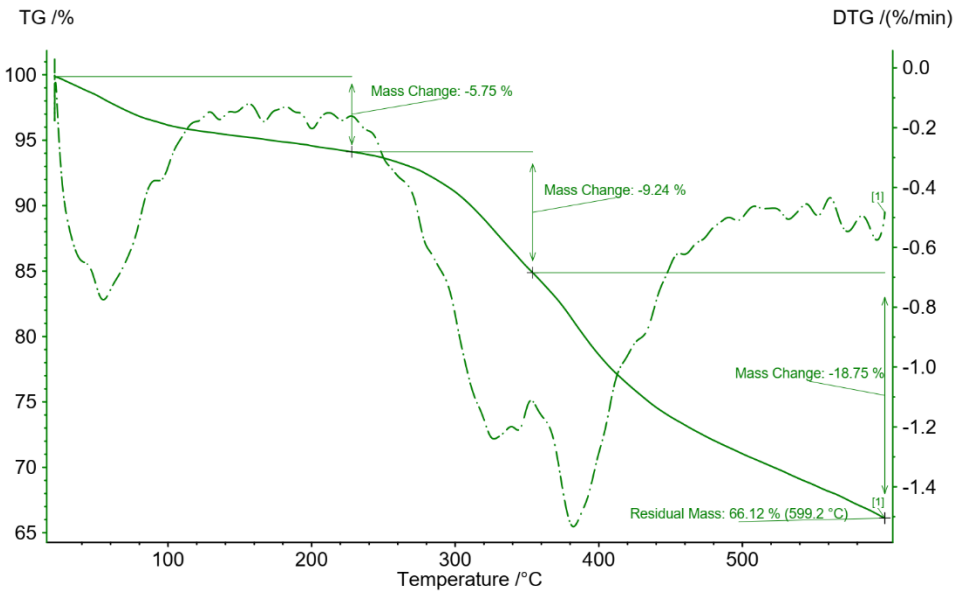

Figure S35. TGA patterns for Cl-HMON-L-A-5

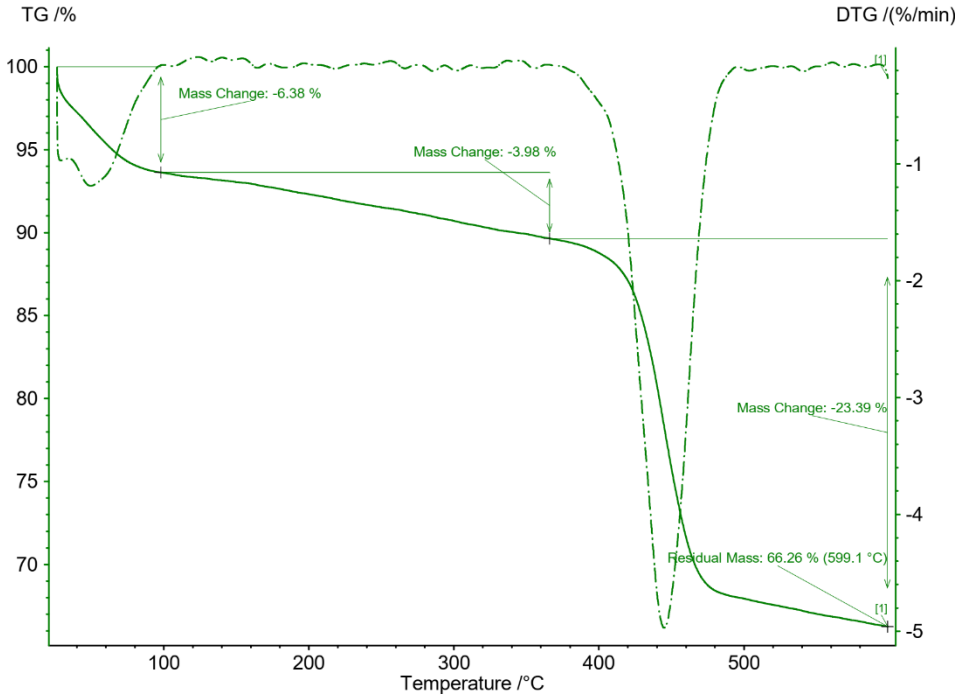

Figure S36. TGA patterns for Cl-HMON-L-B-1

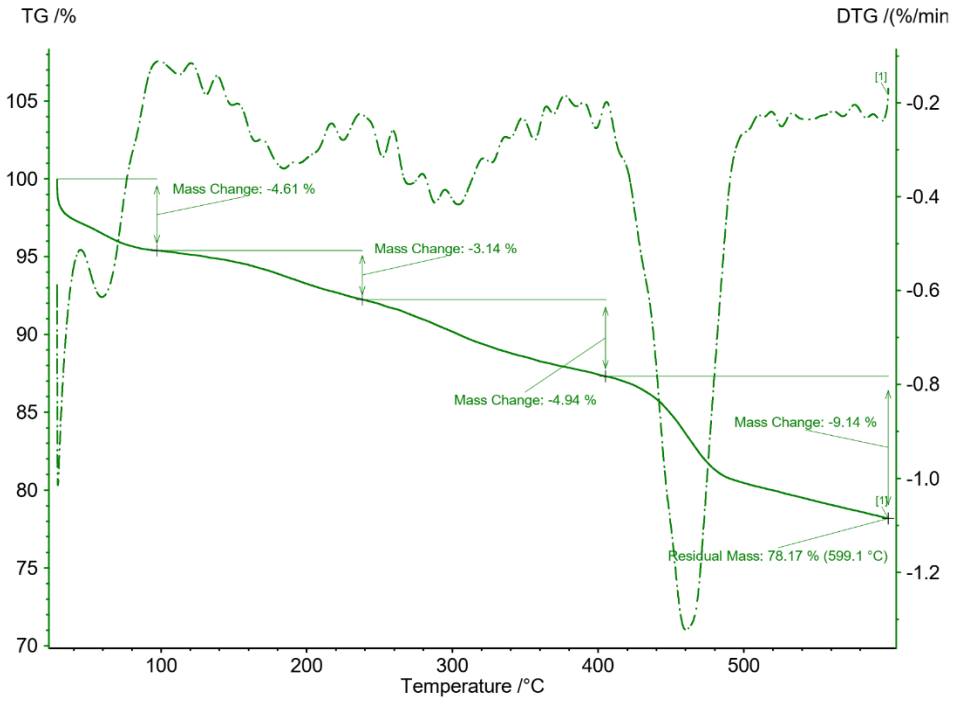

Figure S37. TGA patterns for Cl-HMON-L-B-2.5

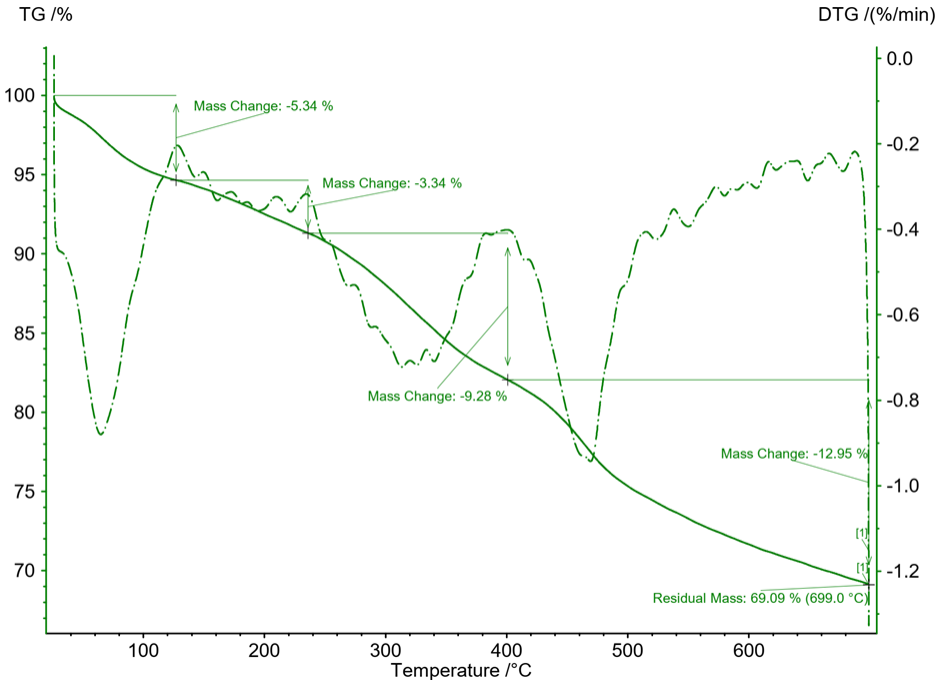

Figure S38. TGA patterns for Cl-HMON-L-C-1

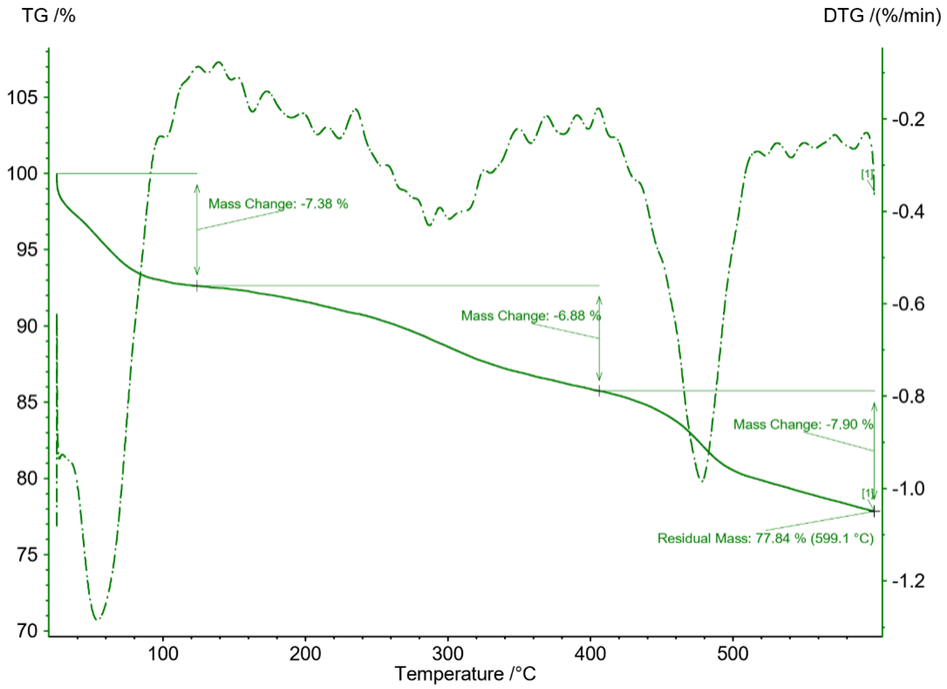

Figure S39. TGA patterns for Cl-HMON-L-C-2.5

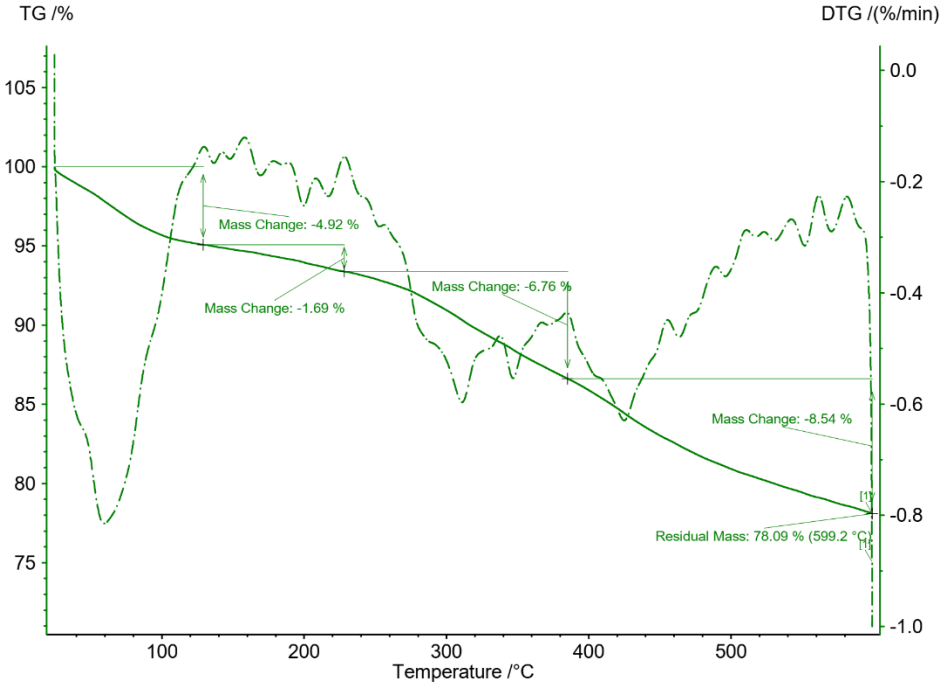

Figure S40. TGA patterns for Cl-HMON-S-D-2.5

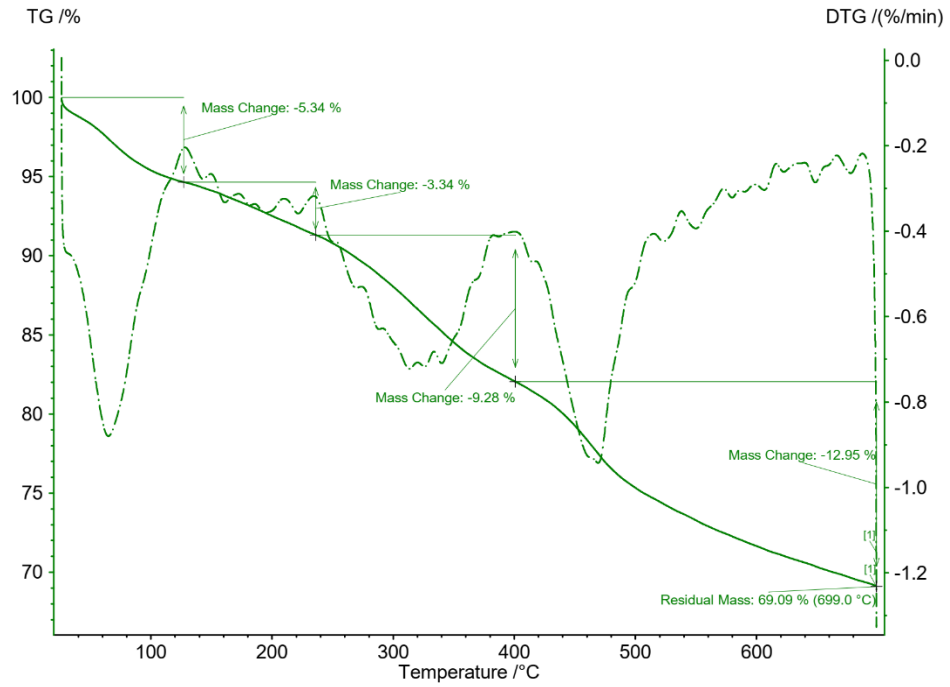

Figure S41. TGA patterns for Cl-HMON-S-D-5

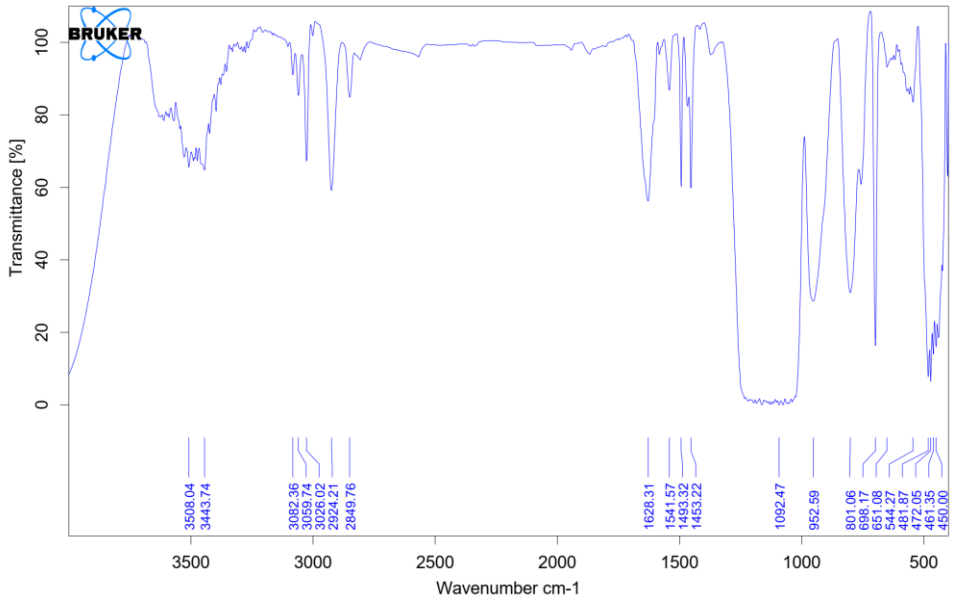

Figure S42. FTIR spectrum for I-HMON-L-B-1

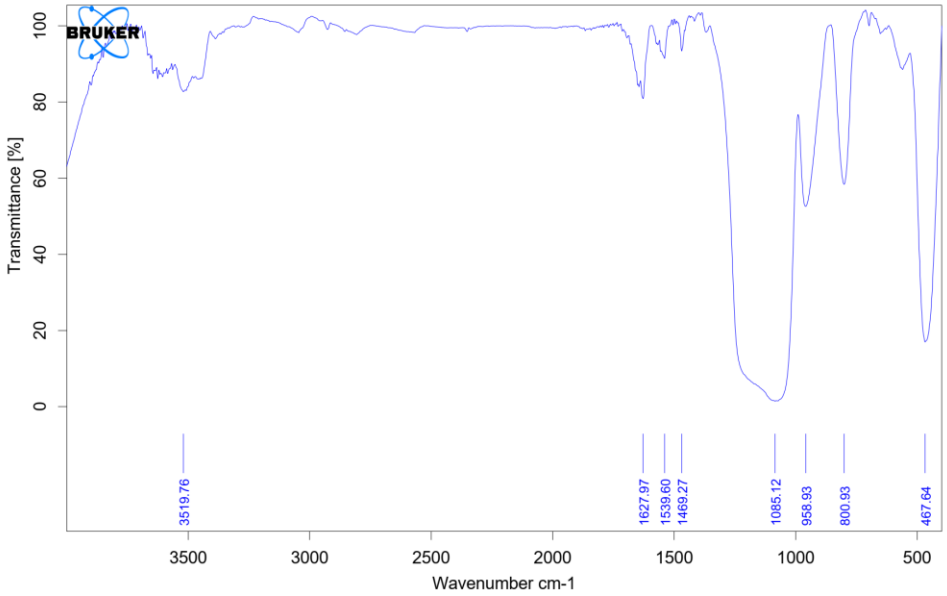

Figure S43. FTIR spectrum for I-HMON-L-C-1

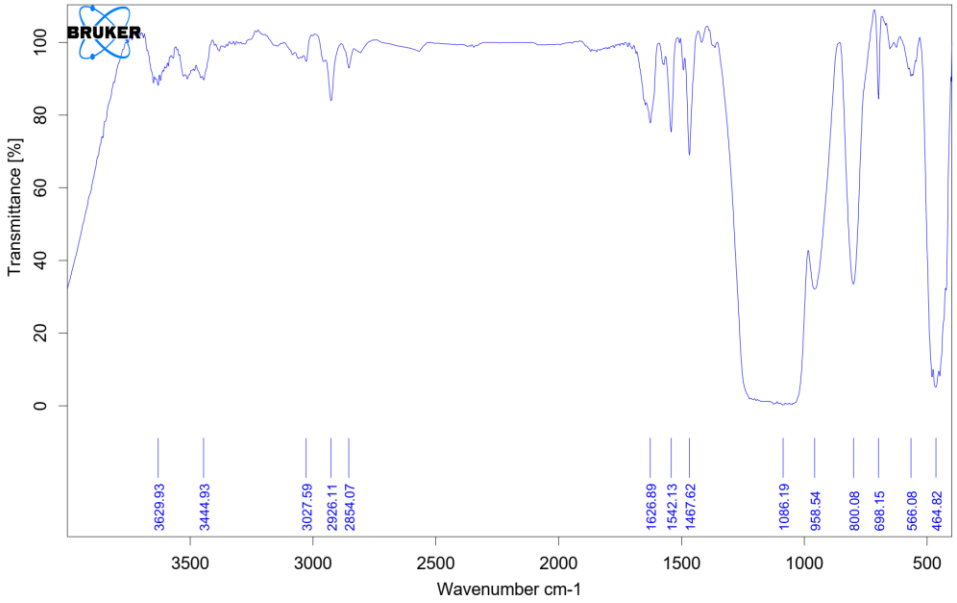

Figure S44. FTIR spectrum for I-HMON-L-C-2.5

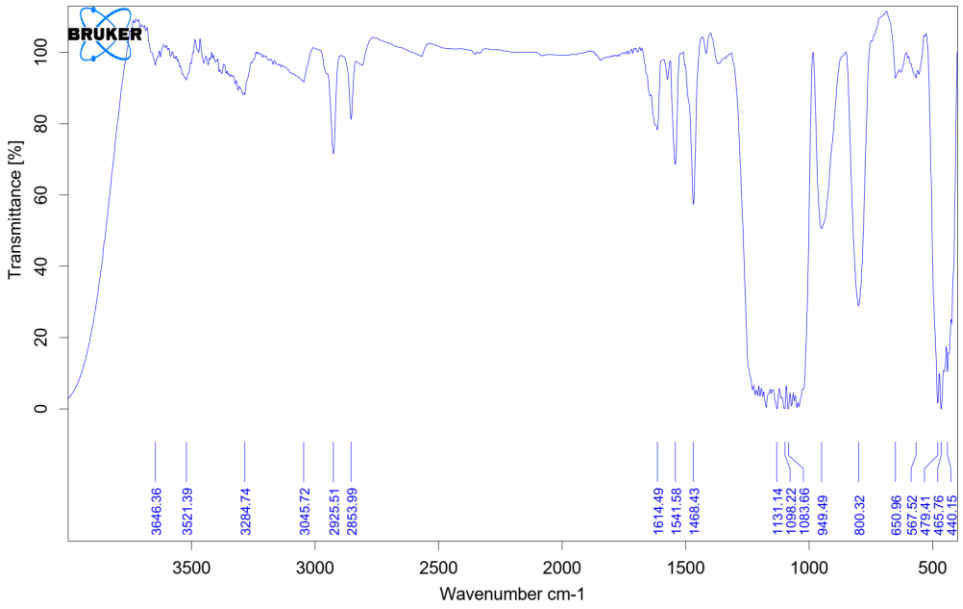

Figure S45. FTIR spectrum for I-HMON-S-D-2.5

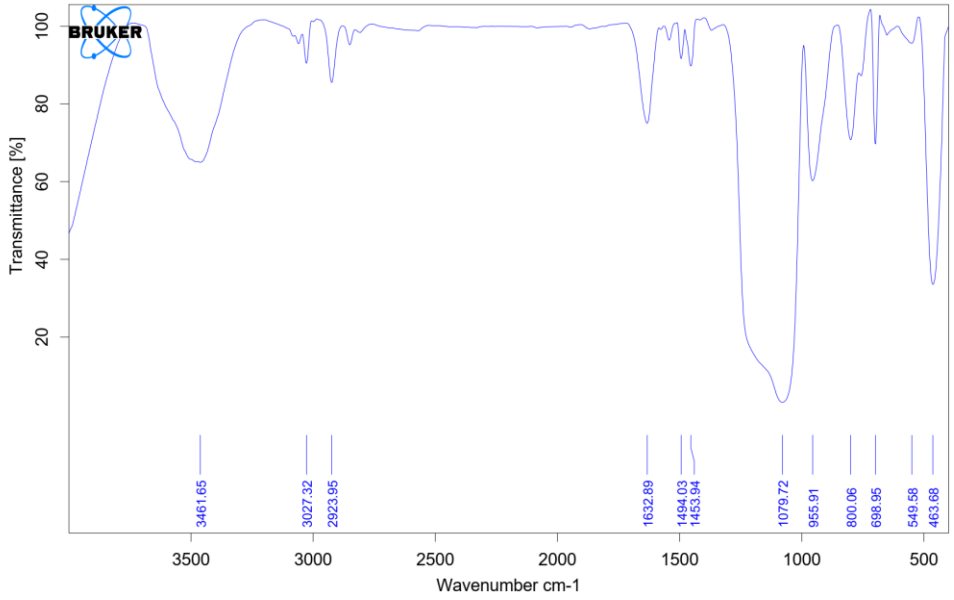

Figure S46. FTIR spectrum for Cl-HMON-L-A-1

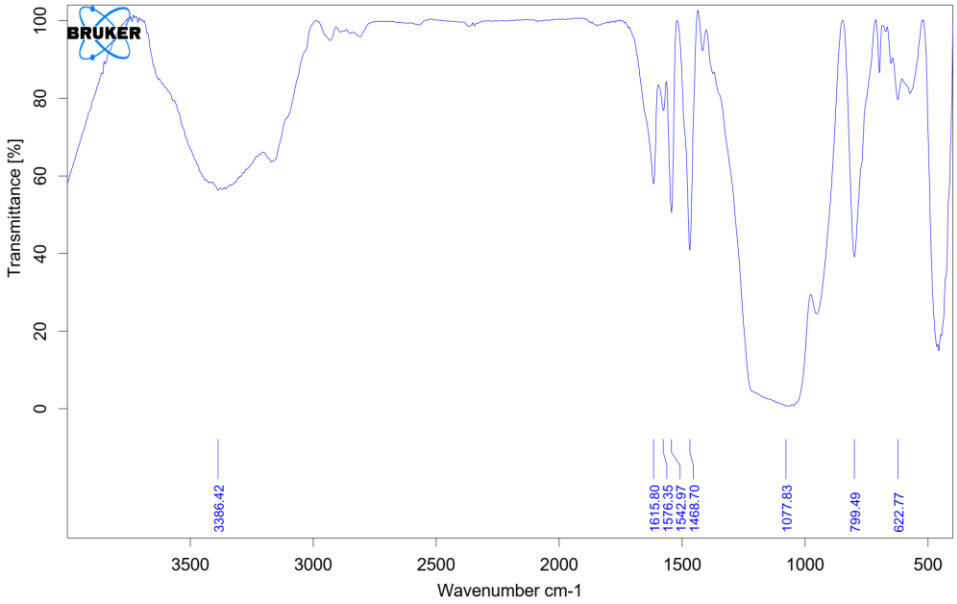

Figure S47. FTIR spectrum for Cl-HMON-L-A-2.5

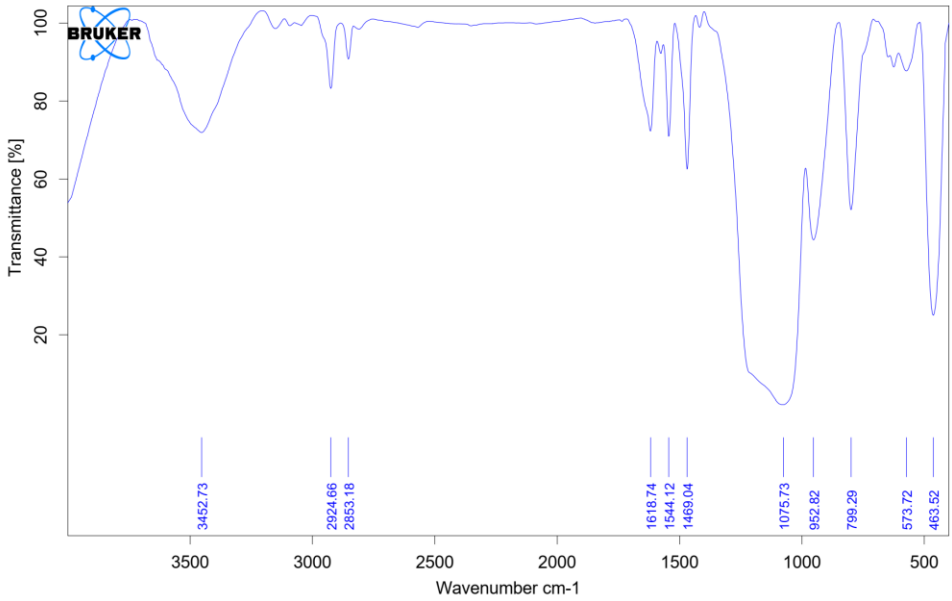

Figure S48. FTIR spectrum for Cl-HMON-L-A-5

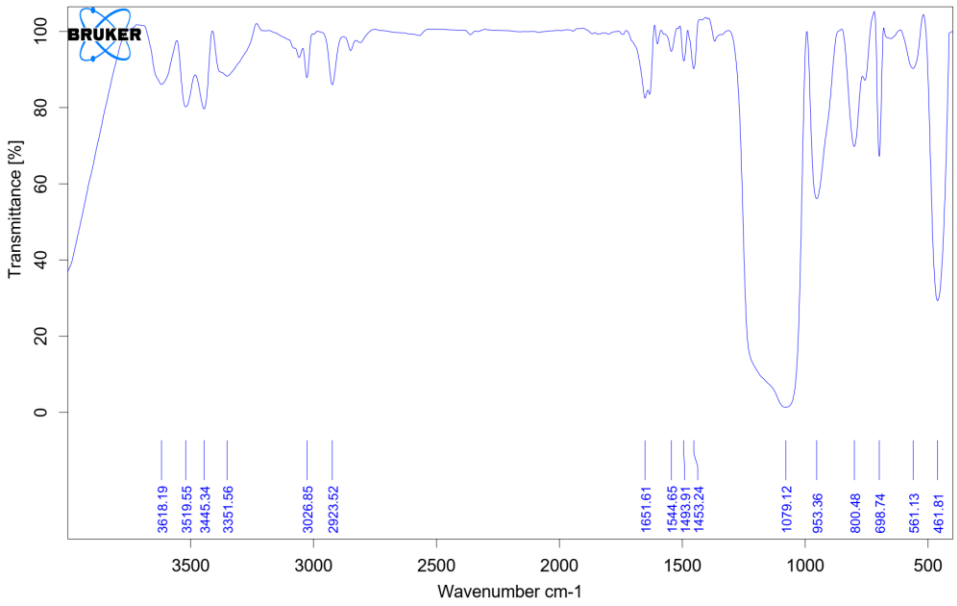

Figure S49. FTIR spectrum for Cl-HMON-L-B-1

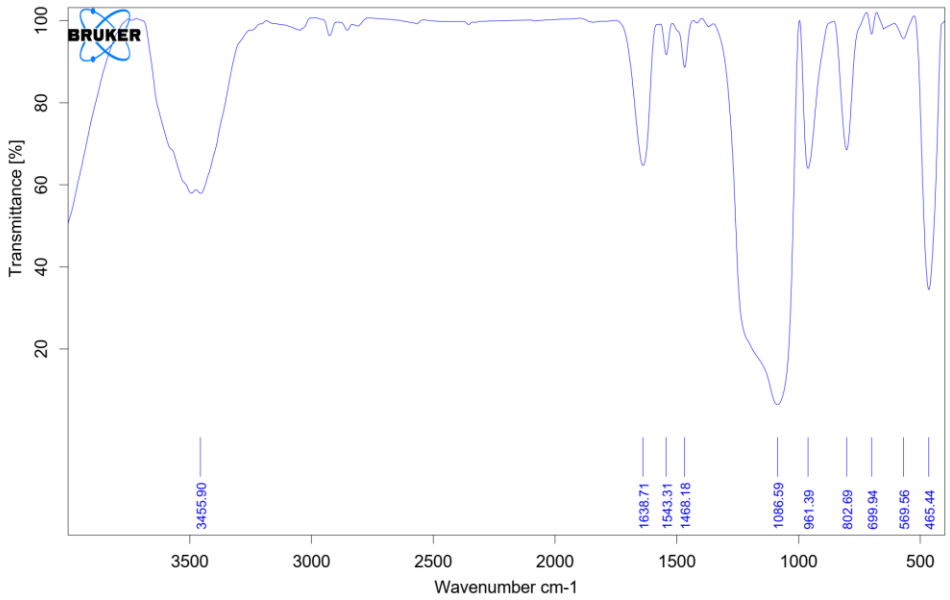

Figure S50. FTIR spectrum for Cl-HMON-L-B-2.5

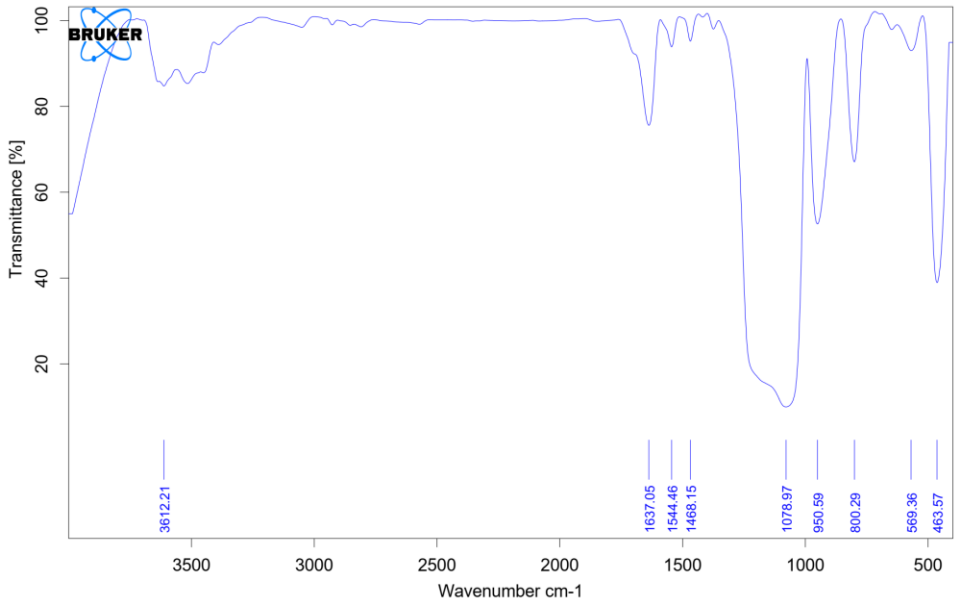

Figure S51. FTIR spectrum for Cl-HMON-L-C-1

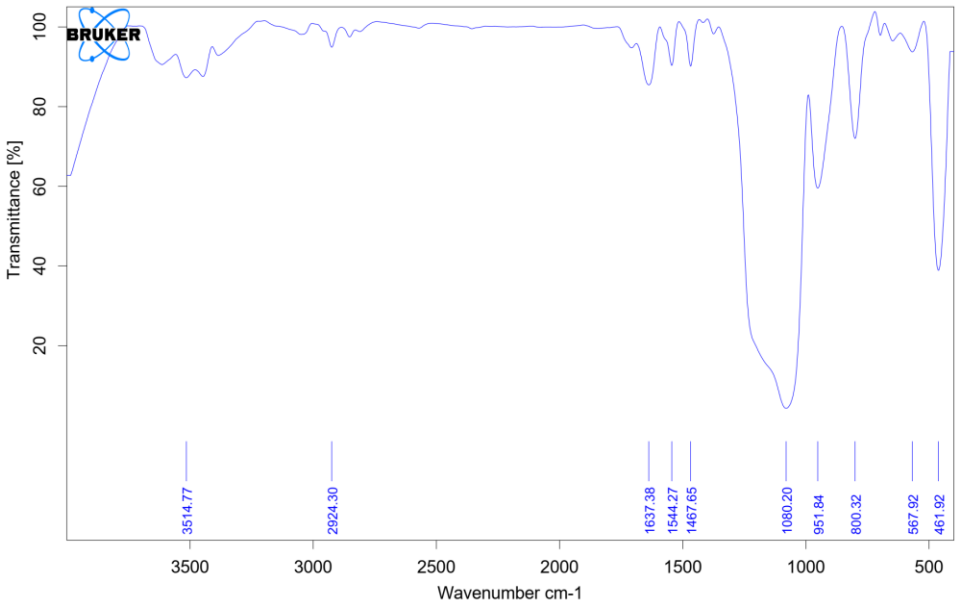

Figure S52. FTIR spectrum for Cl-HMON-L-C-2.5

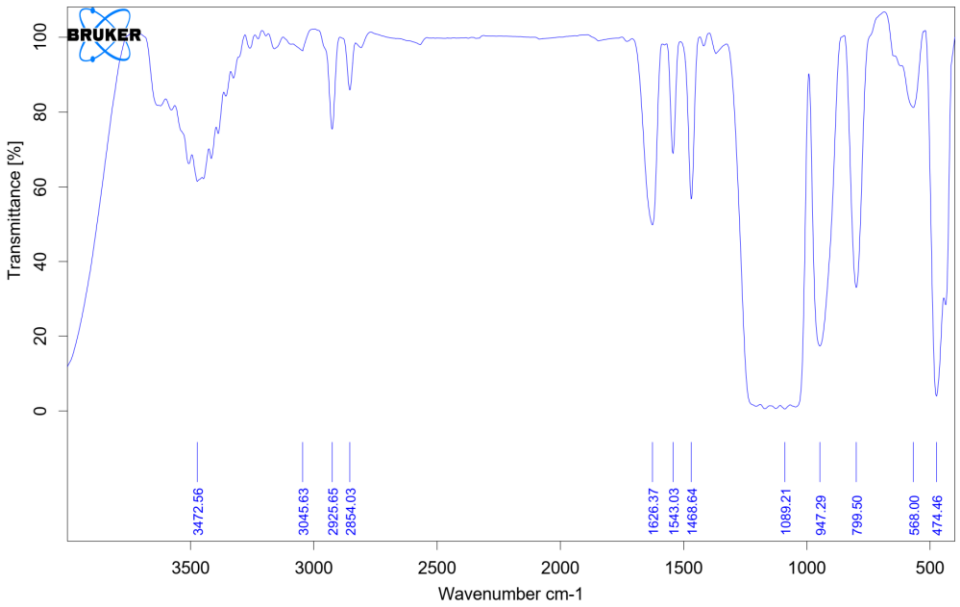

Figure S53. FTIR spectrum for Cl-HMON-S-D-2.5

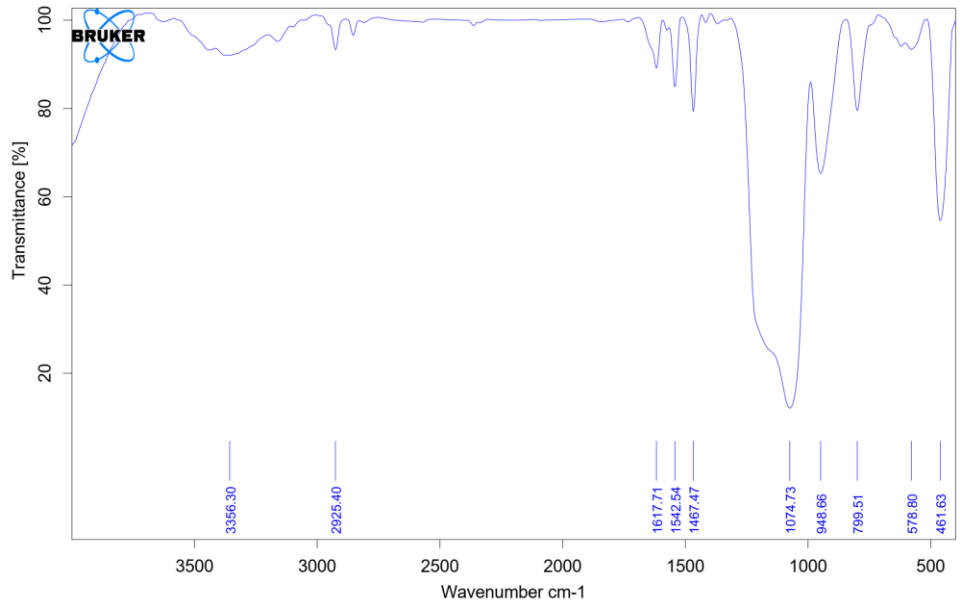

Figure S54. FTIR spectrum for Cl-HMON-S-D-5

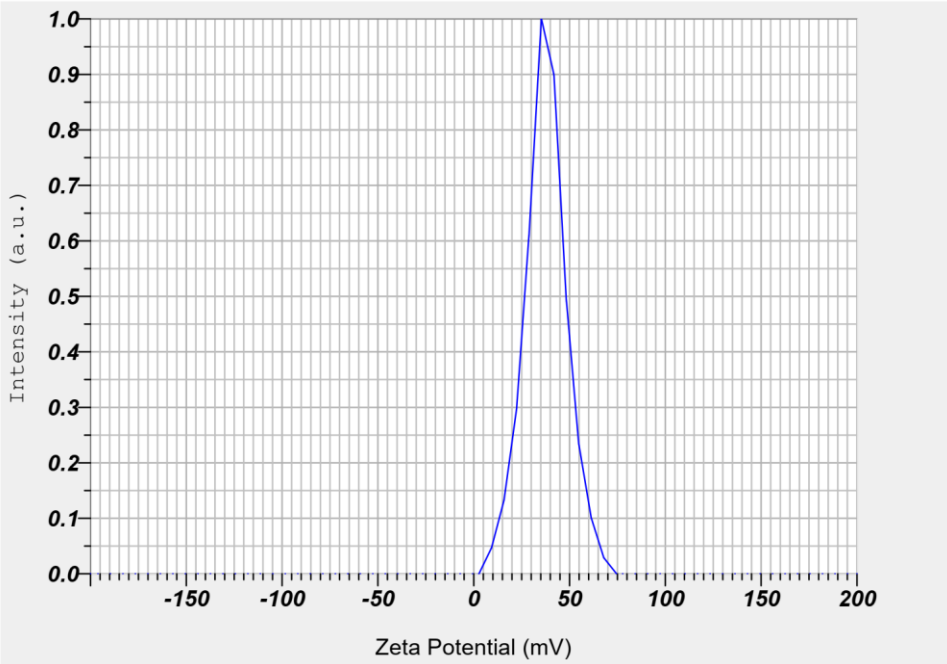

Figure S55. Zeta potential graph for I-HMON-L-C-2.5

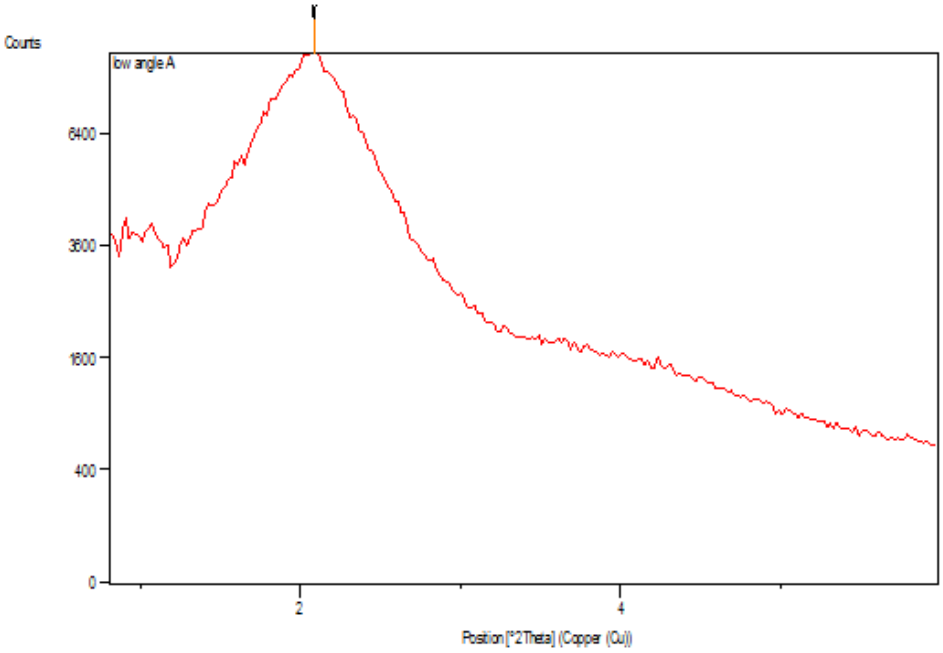

Figure S56. PXRD patterns for I-HMON-L-B-1

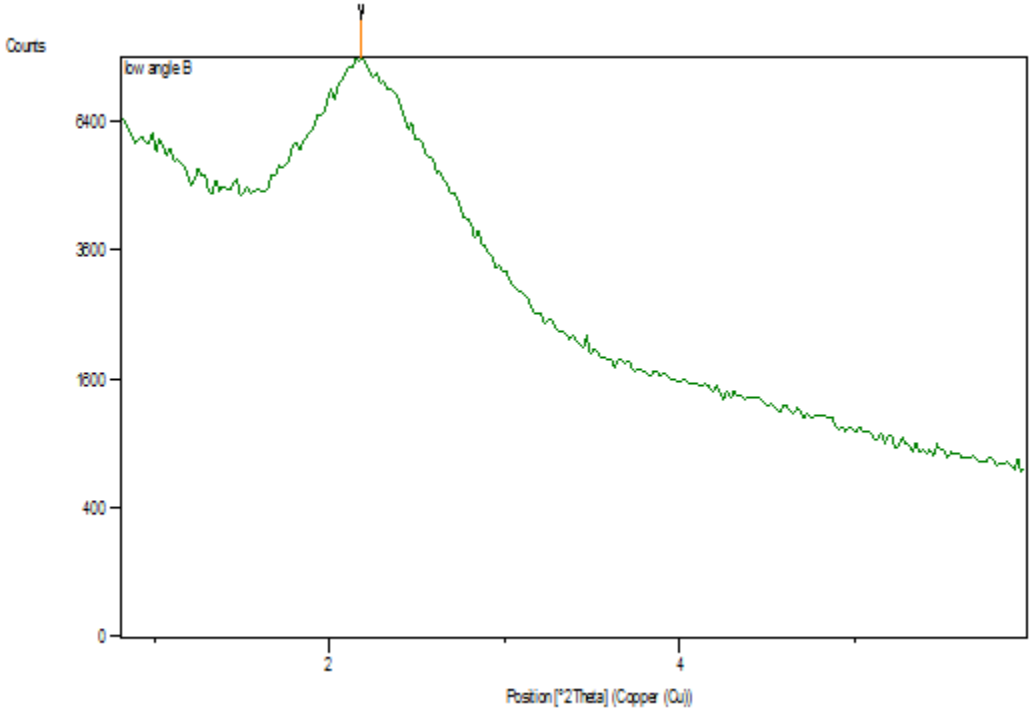

Figure S57. PXRD patterns for I-HMON-L-C-1

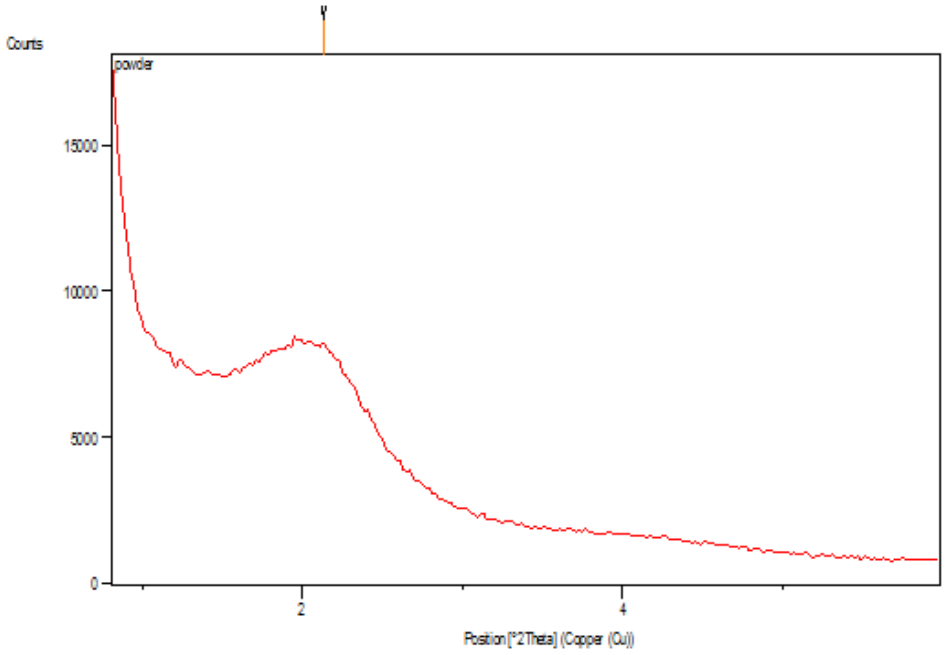

Figure S58. PXRD patterns for I-HMON-L-C-2.5

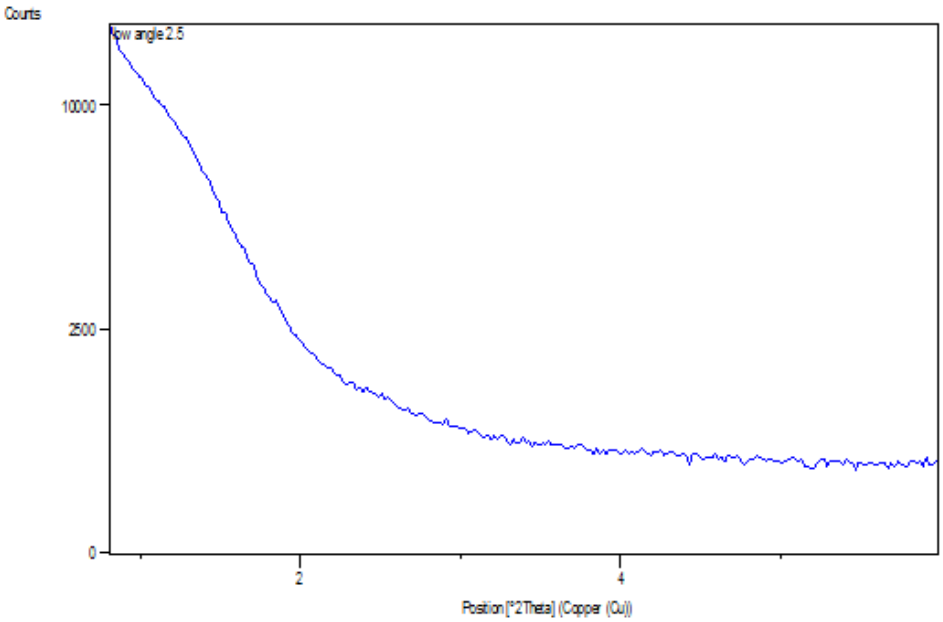

Figure S59. PXRD patterns for I-HMON-S-D-2.5

Figure S60. ^{29}Si CP-MAS NMR for Cl-HMON-L-B-1

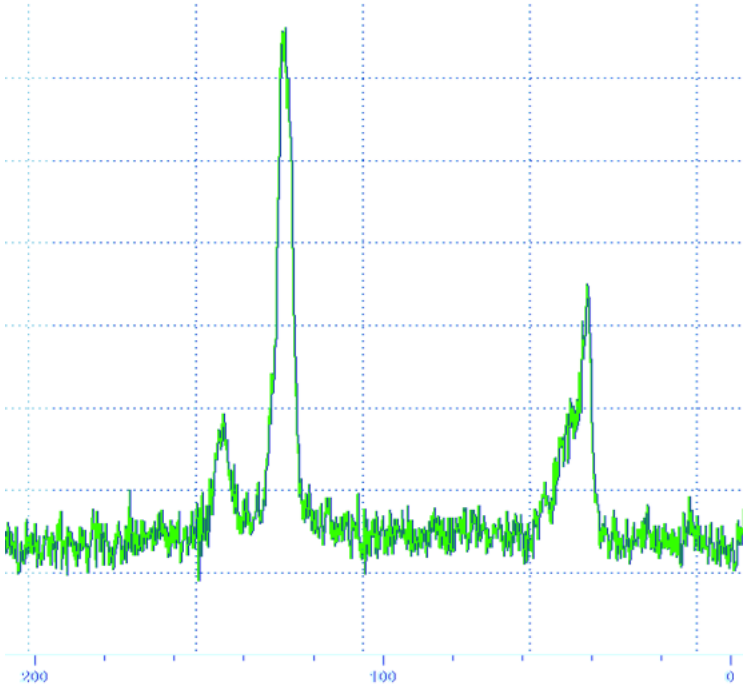

Figure S61. ^{13}C CP-MAS NMR for Cl-HMON-L-B-1

Figure S62. ^{29}Si CP-MAS NMR for Cl-HMON-L-C-1

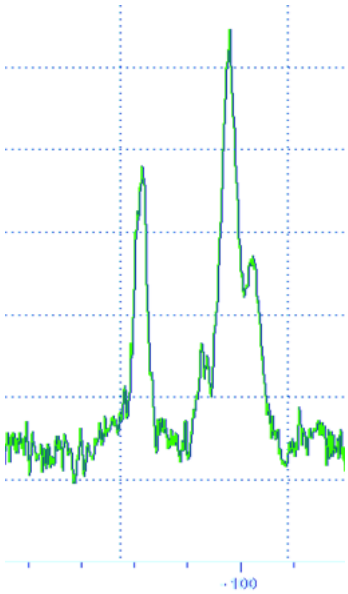

Figure S63. ^{29}Si CP-MAS NMR for Cl-HMON-S-D-2.5

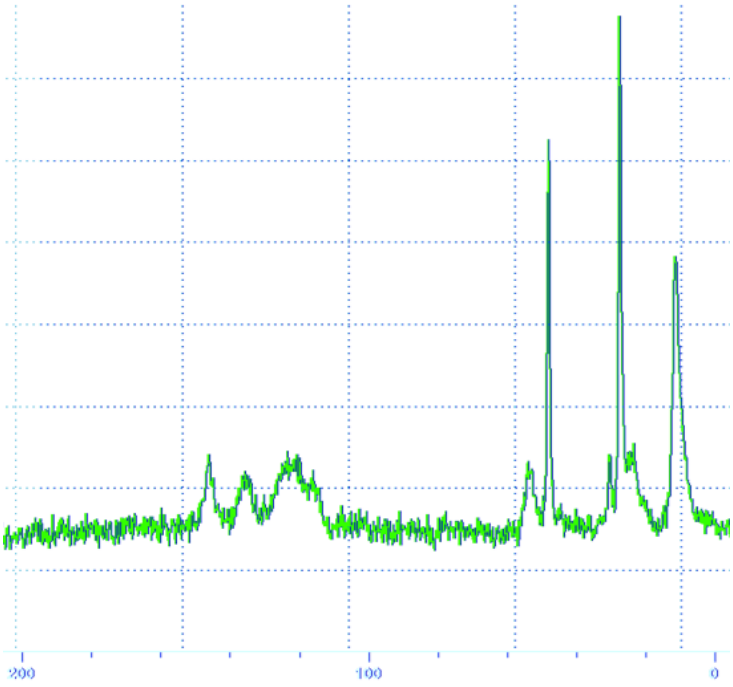

Figure S64. ^{13}C CP-MAS NMR for Cl-HMON-S-D-2.5

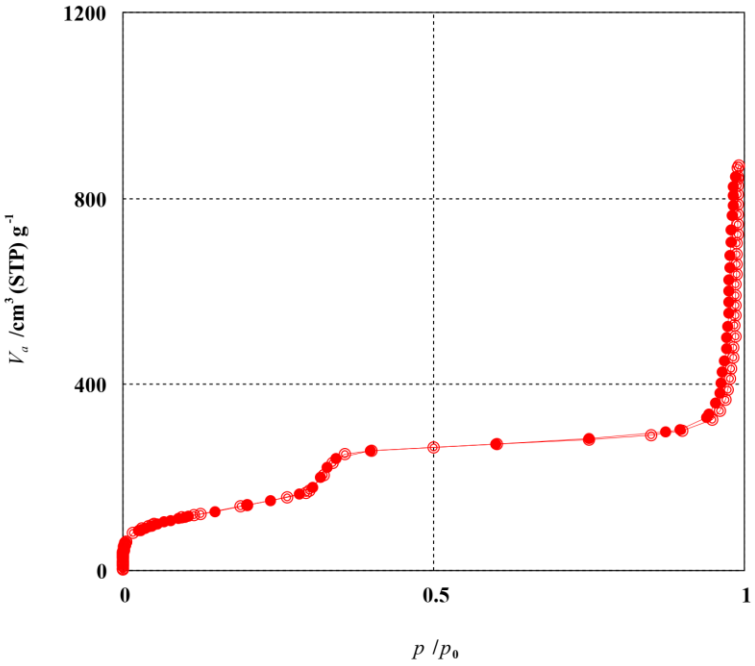

Figure S65. Nitrogen isotherm for I-MON

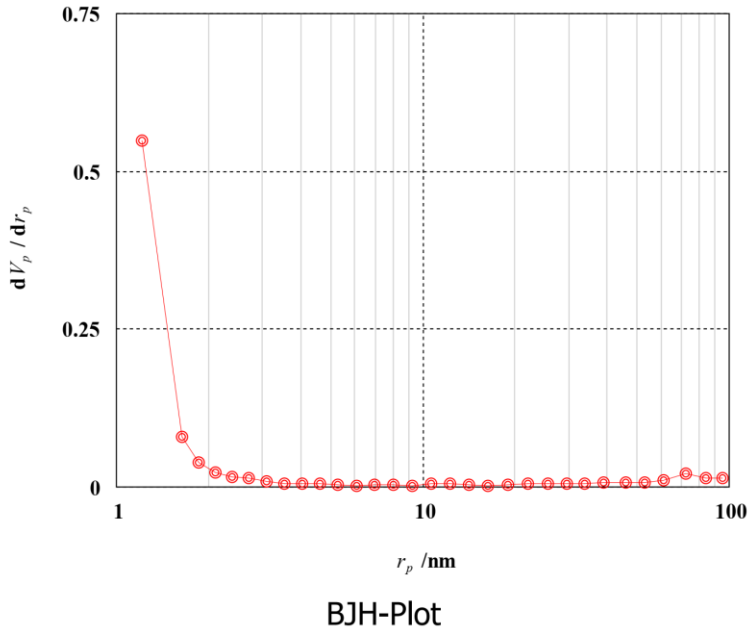

Figure S66. BJH pore side distribution for I-MON

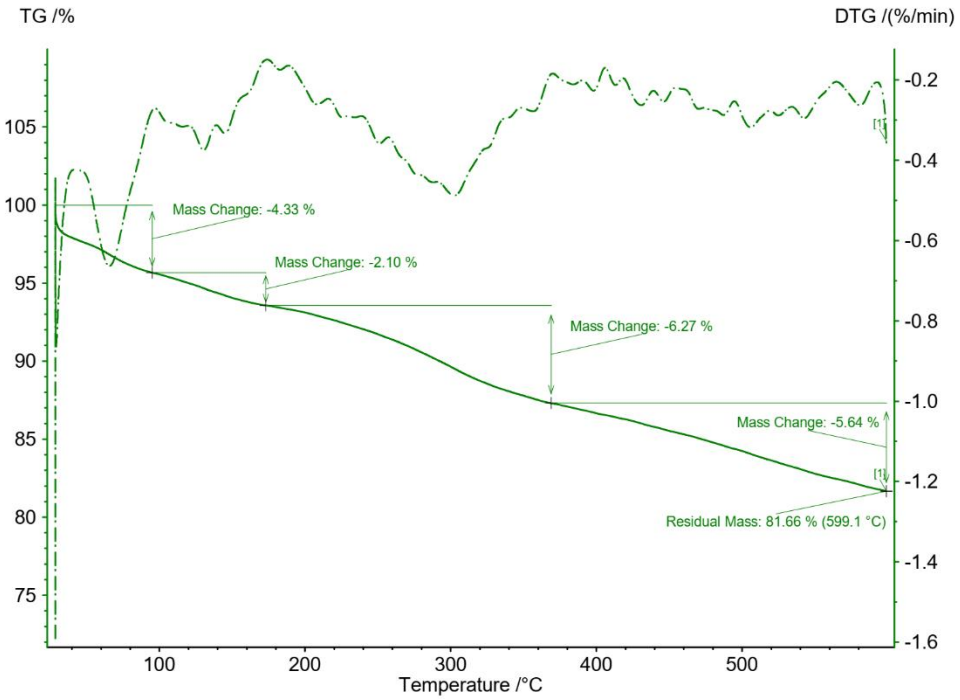

Figure S67. TGA pattern for I-MON

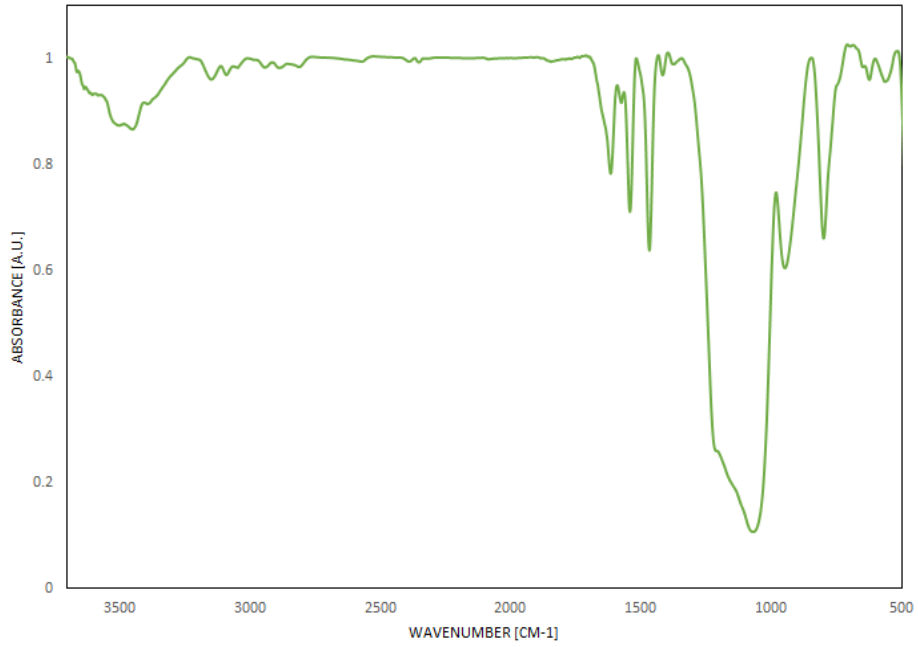

Figure S68. FTIR spectrum for I-MON

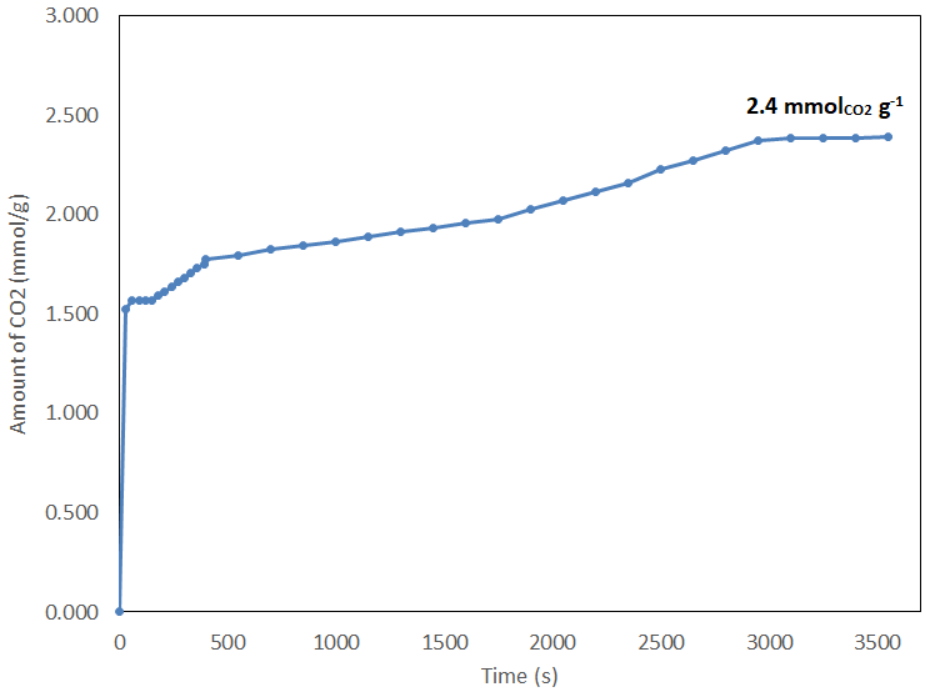

Figure S69. CO_2 adsorption capacity for I-HMON-L-C-2.5

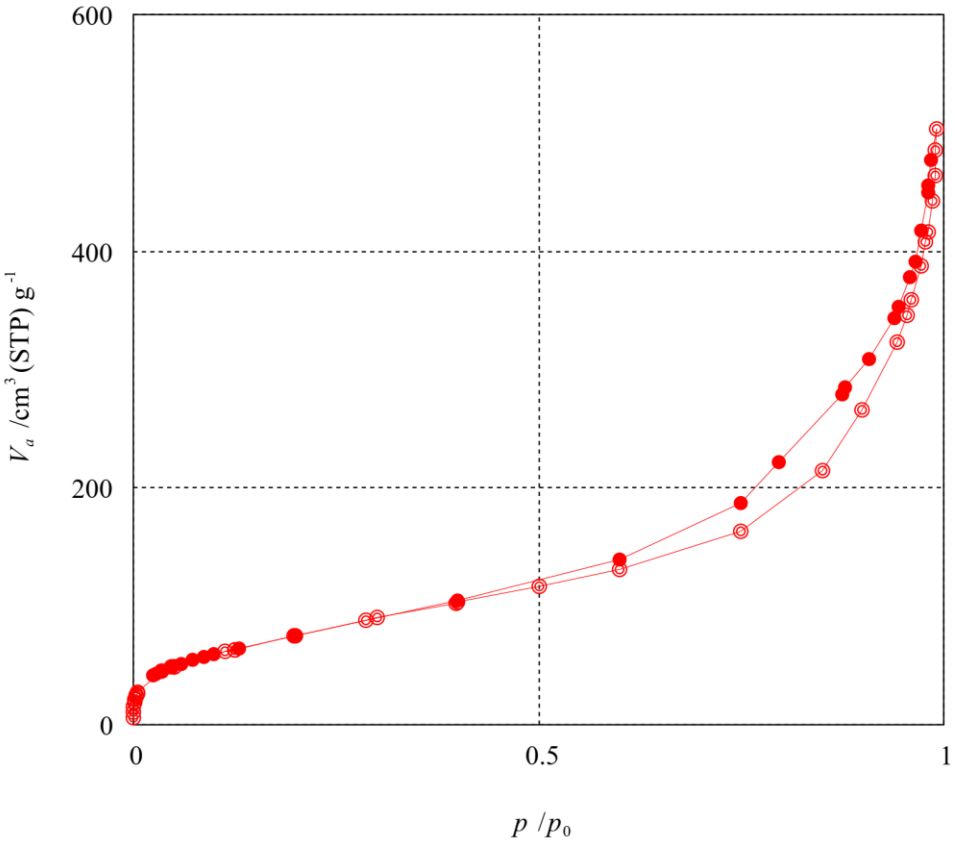

Figure S70. Nitrogen isotherm for Re-used I-HMON-L-C-2.5

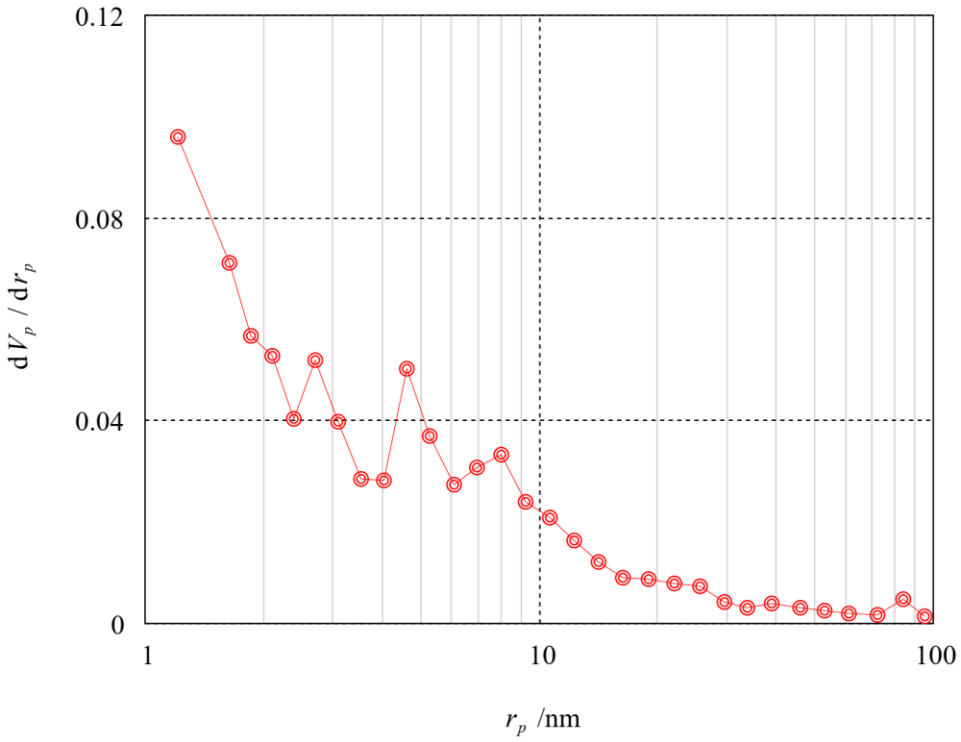

Figure S71. BJH pore side distribution for Re-used I-HMON-L-C-2.5

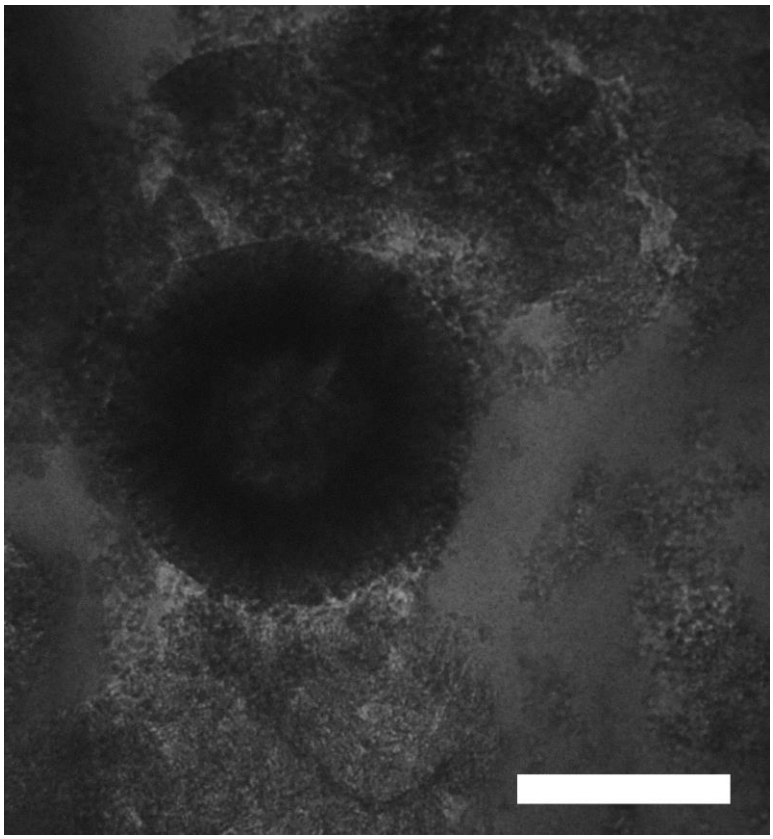

Figure S72. TEM image for Reused I-HMON-L-C-2.5, scale bar 200 nm.

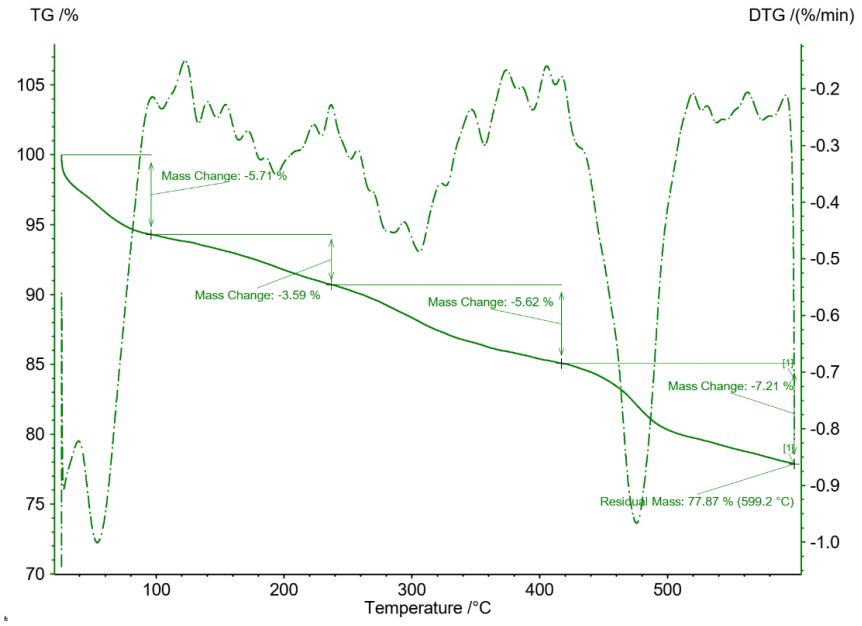

Figure S73. TGA pattern for Reused-I-HMON-L-C-2.5

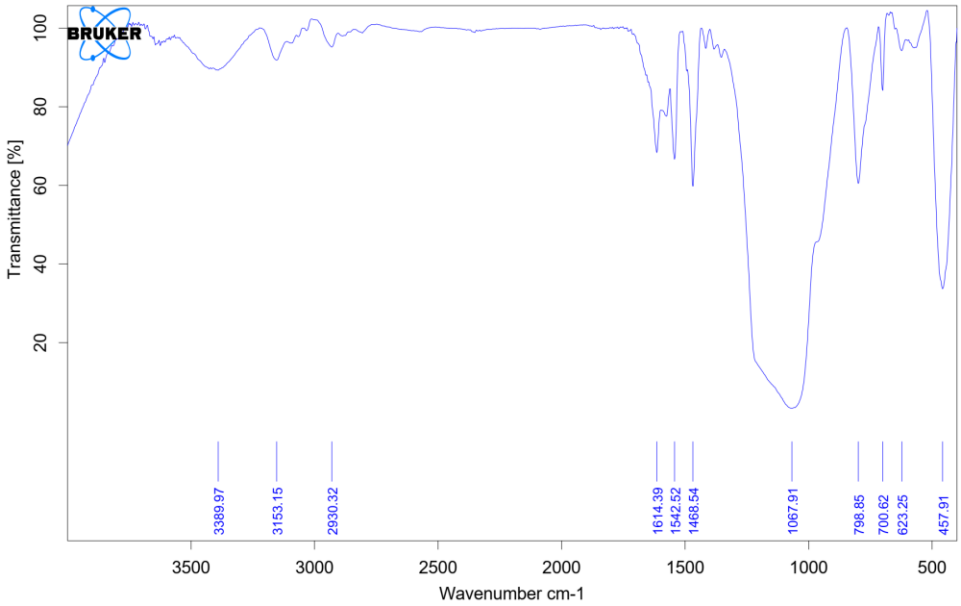

Figure S74. FTIR spectrum for Reused I-HMON-L-C-2.5

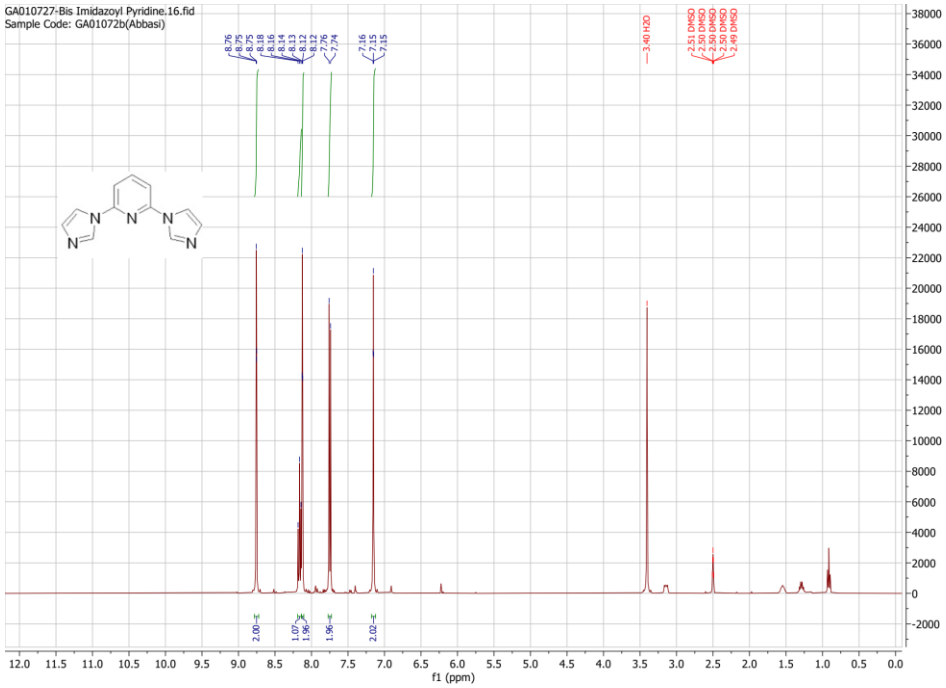

Figure S75. ^{1}H-NMR spectrum for 2,6-bis(1-imidazoyl-pyridine in DMSO-d_6

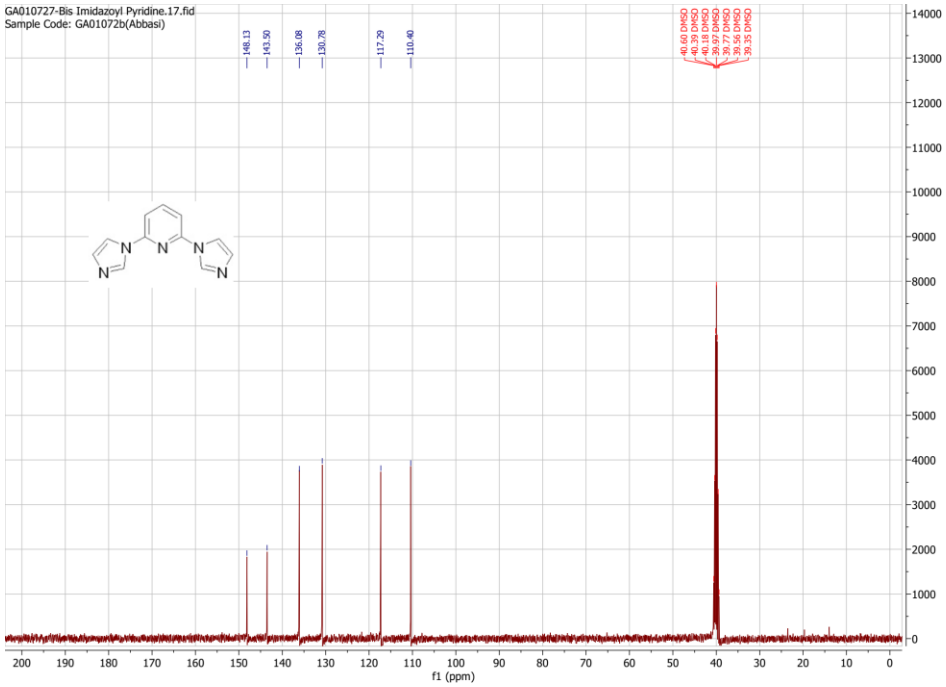

Figure S76. ^{13}C-NMR spectrum for 2,6-bis(1-imidazoyl-pyridine in DMSO-d_6

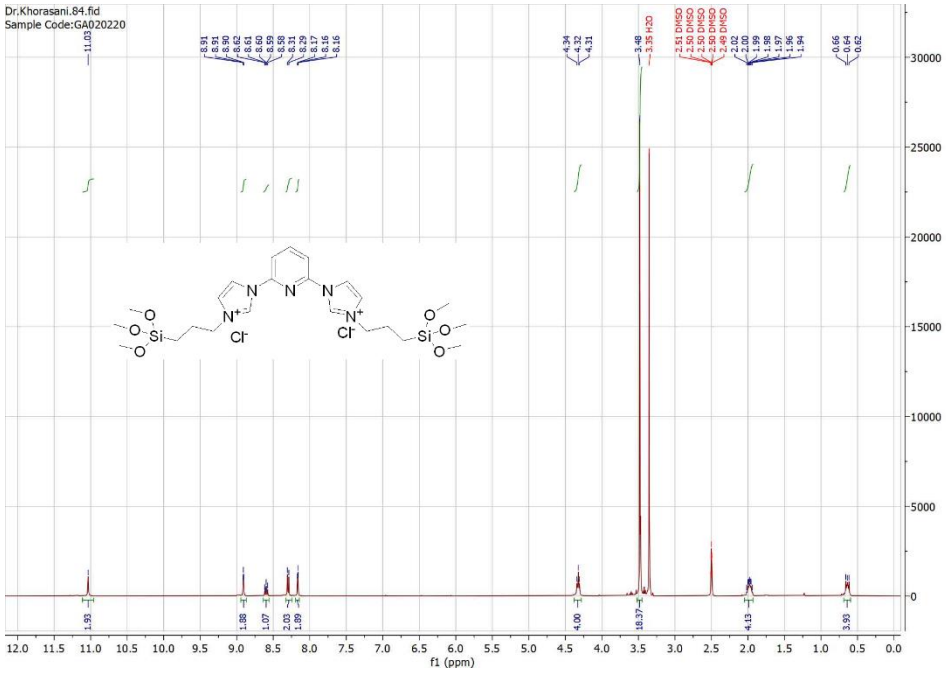

Figure S77. ^{1}H-NMR spectrum for organosilica precursor in DMSO-d_6

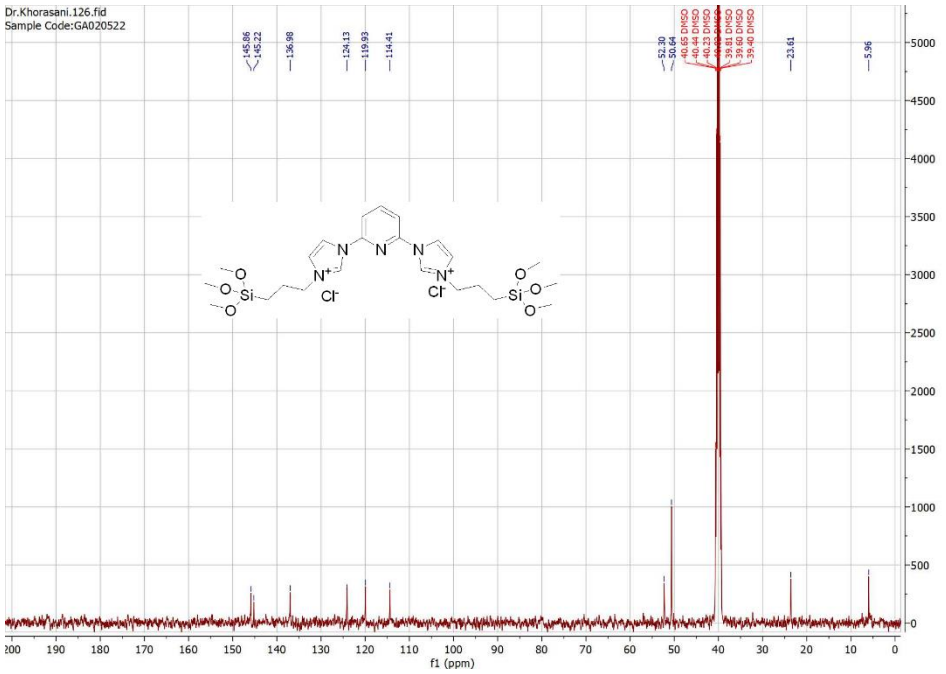

Figure S78. ^{13}C-NMR spectrum for organosilica precursor in DMSO-d_6

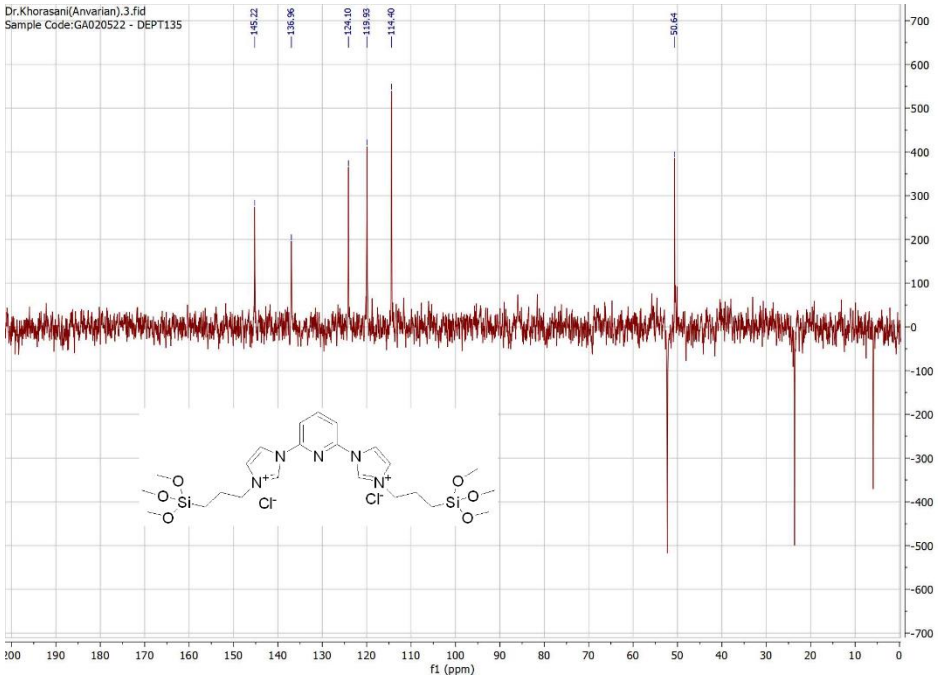

Figure S79. DEPT135 spectrum for organosilica precursor in DMSO-d_6

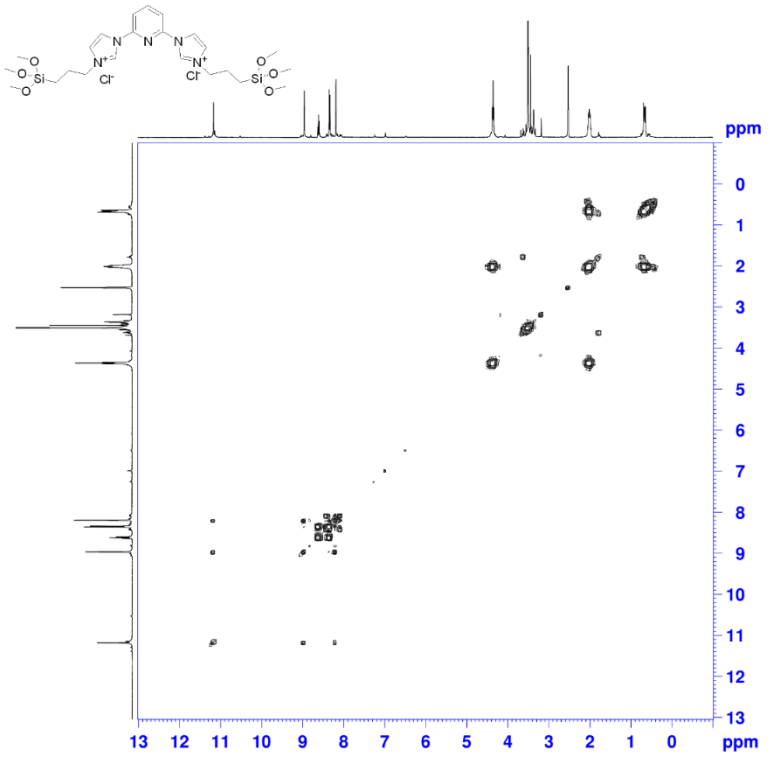

Figure S80. COSY spectrum for organosilica precursor in DMSO-d_6

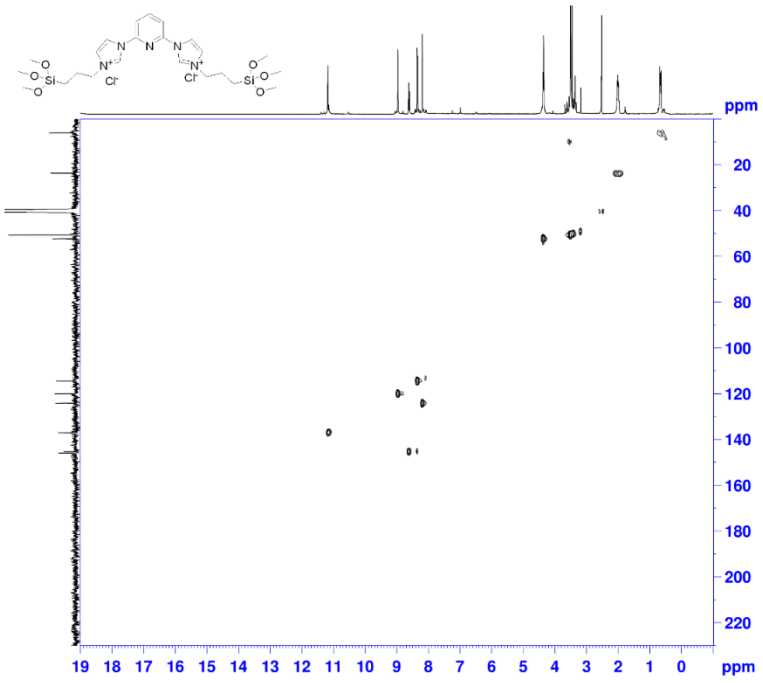

Figure S81. HSQC spectrum for organosilica precursor in DMSO-d_6

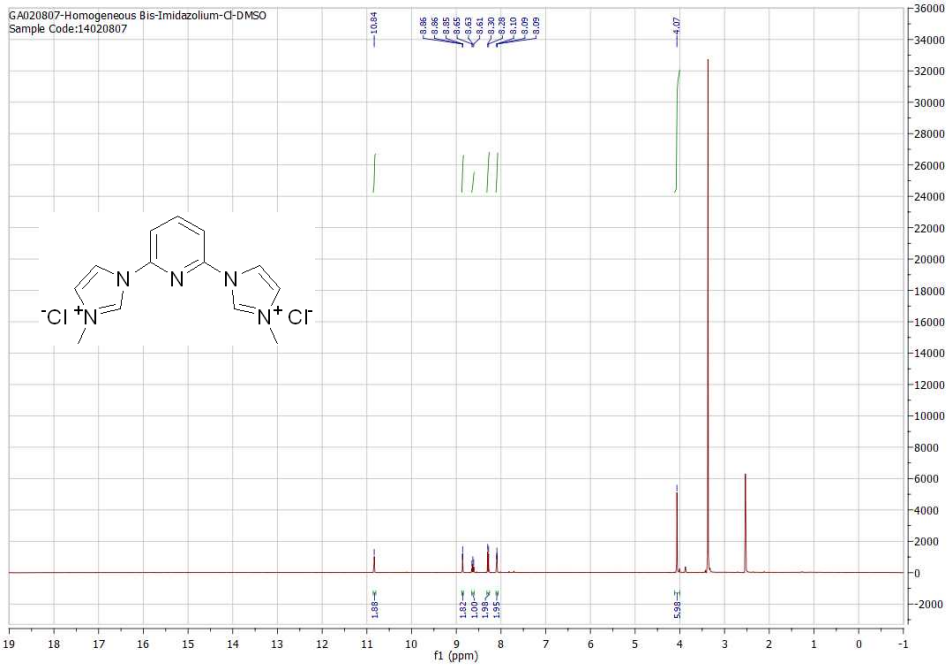

Figure S82. ^{1}H-NMR spectrum for 2,6-bis-(N-methyl imidazolium) pyridine chloride in DMSO-d_6

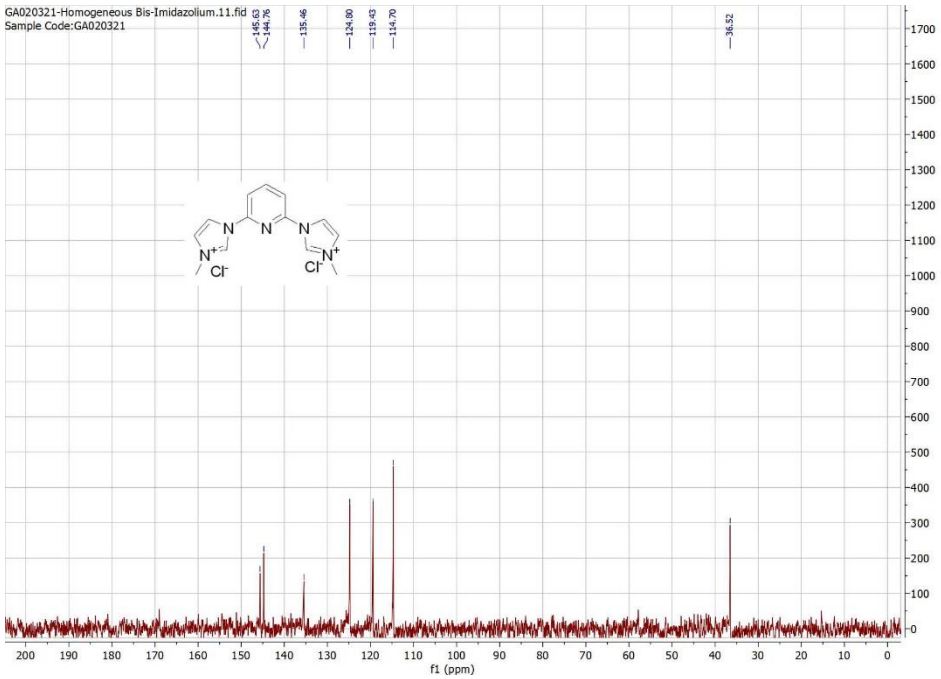

Figure S83. ^{13}C-NMR spectrum for 2,6-bis-(N-methyl imidazolium) pyridine chloride in D_2O

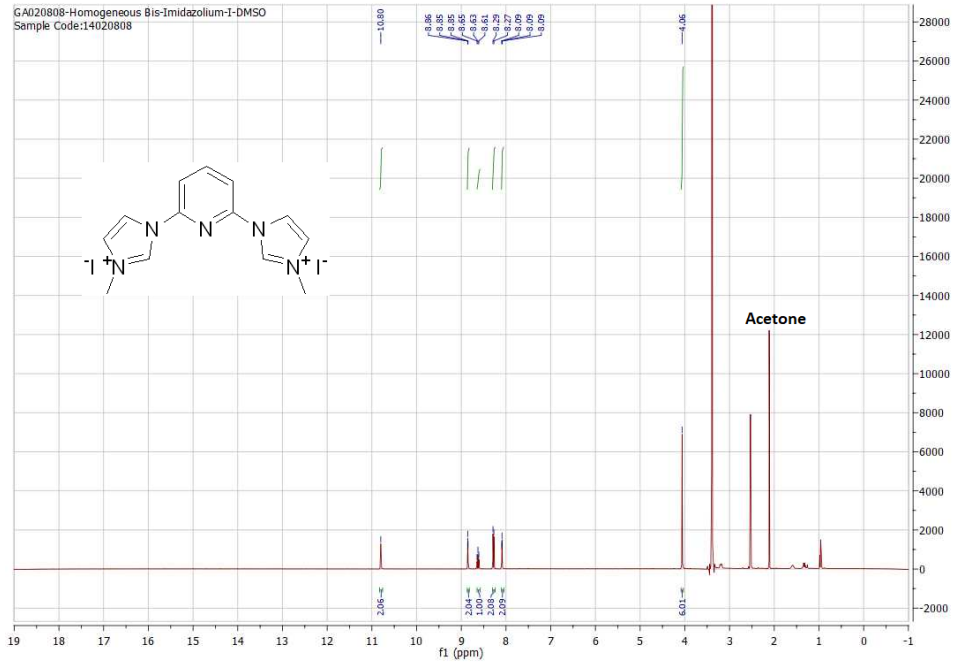

Figure S84. ^{1}H-NMR spectrum for 2,6-bis-(N-methyl imidazolium) pyridine iodide in DMSO-d_6

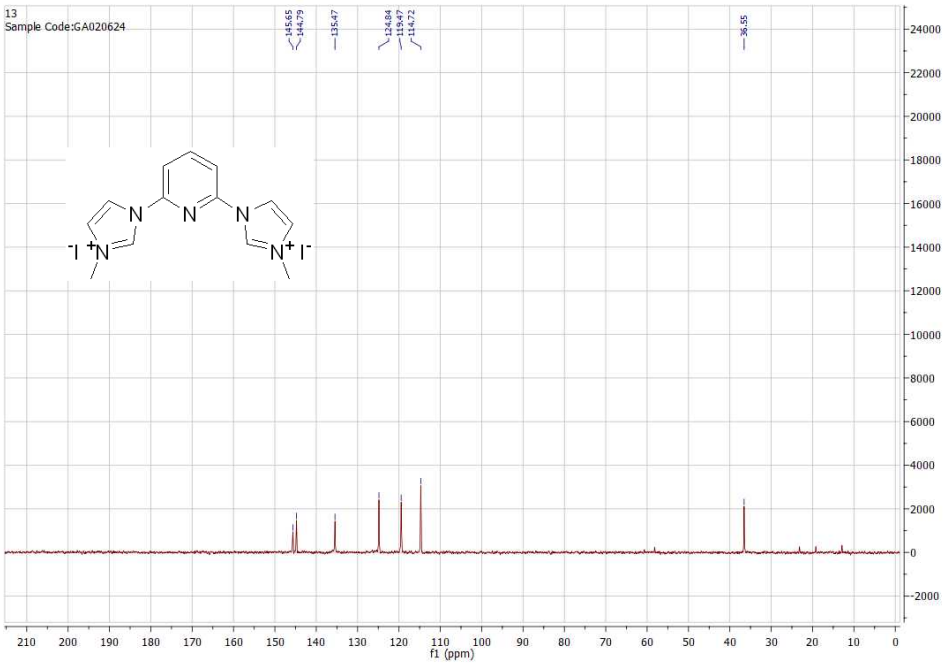

Figure S85. ^{13}C-NMR spectrum for 2,6-bis-(N-methyl imidazolium) pyridine iodide in D_2O

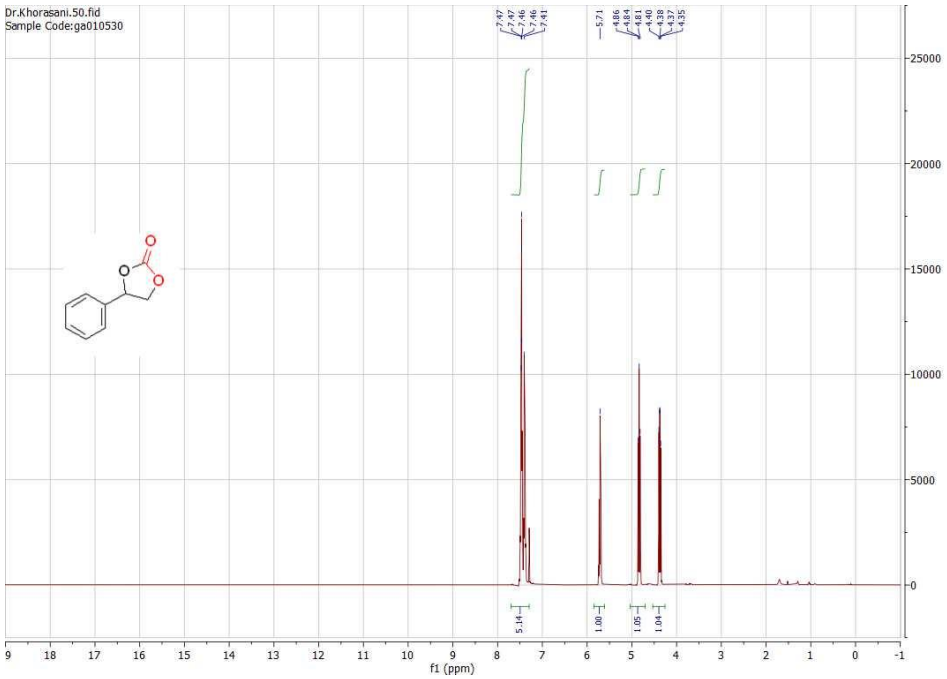

Figure S86. ^{1}H-NMR spectrum for styrene carbonate in $CDCl_3$ as solvent.

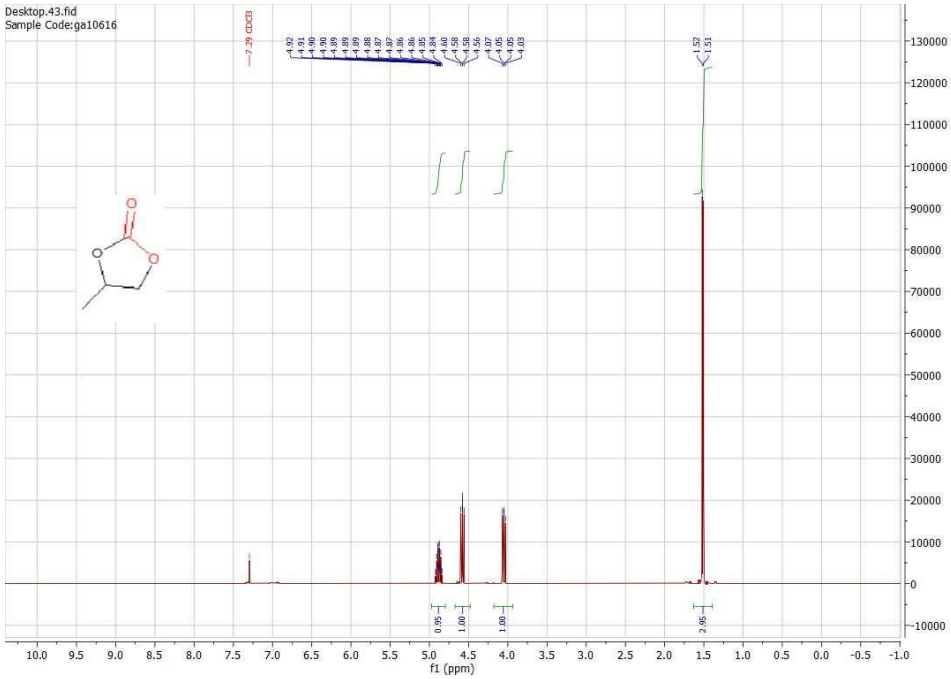

Figure S87. ^{1}H-NMR spectrum for propylene carbonate in $CDCl_3$ as solvent.

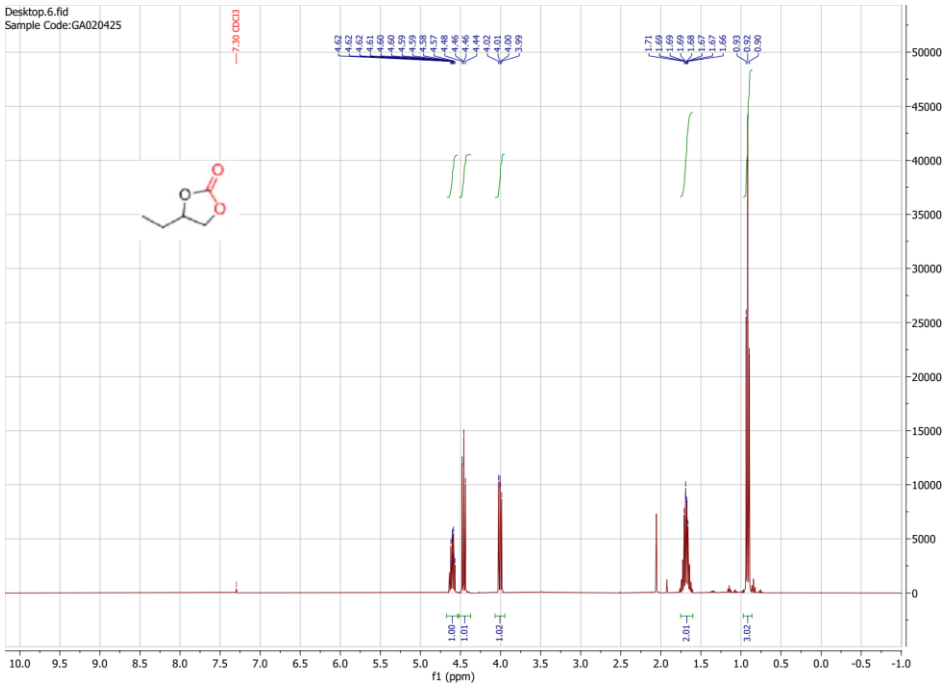

Figure S88. ^{1}H-NMR spectrum for 1,2-butylene carbonate in $CDCl_3$ as solvent

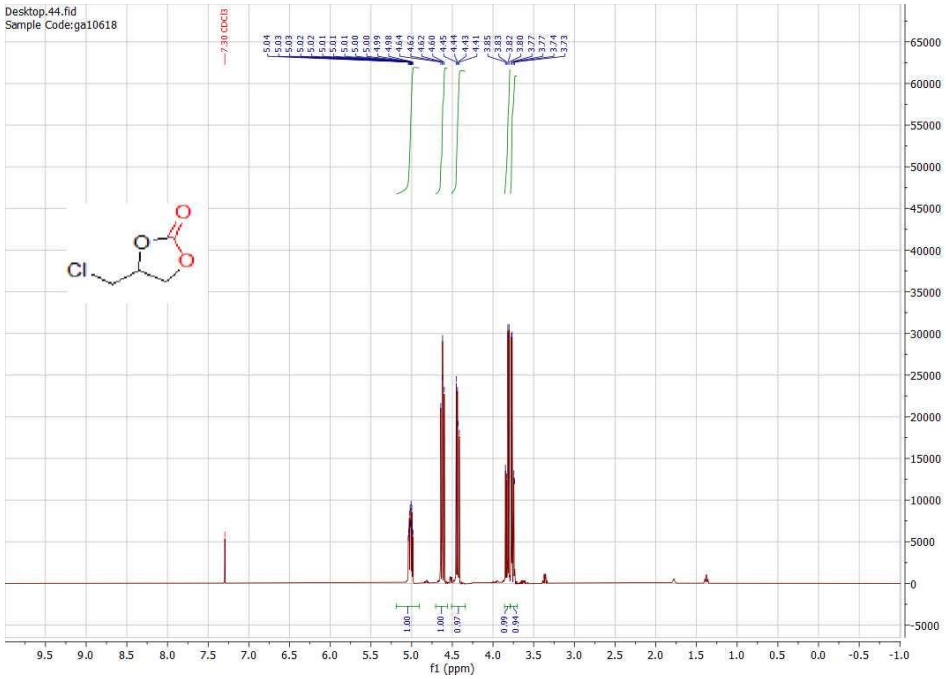

Figure S89. ^{1}H-NMR spectrum for (Chloromethyl)ethylene carbonate in $CDCl_3$ as solvent.

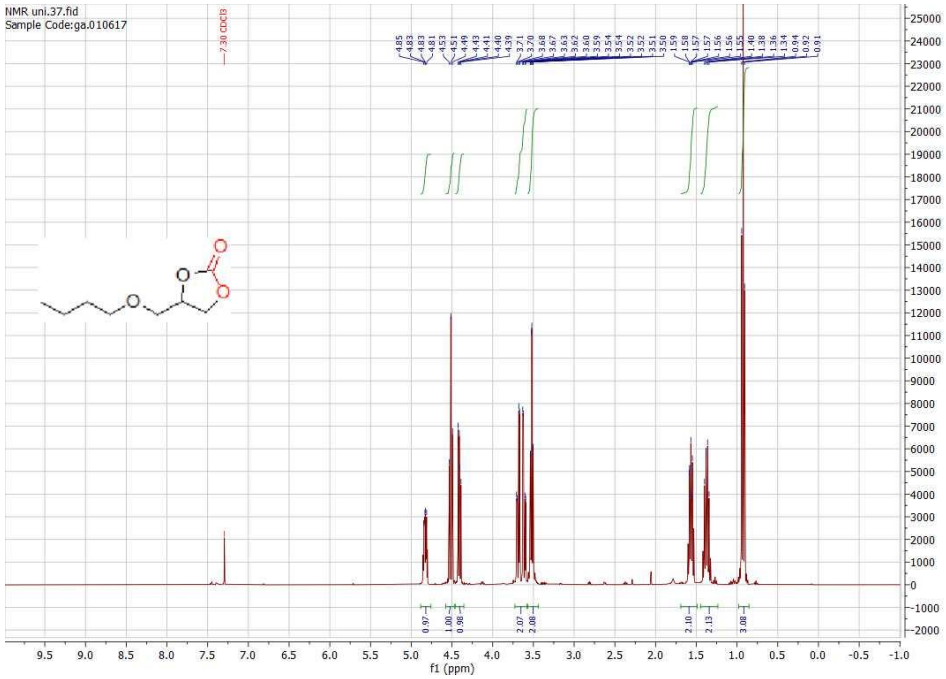

Figure S90. ^{1}H-NMR spectrum for (butoxymethyl)ethylene carbonate in $CDCl_3$ as solvent.

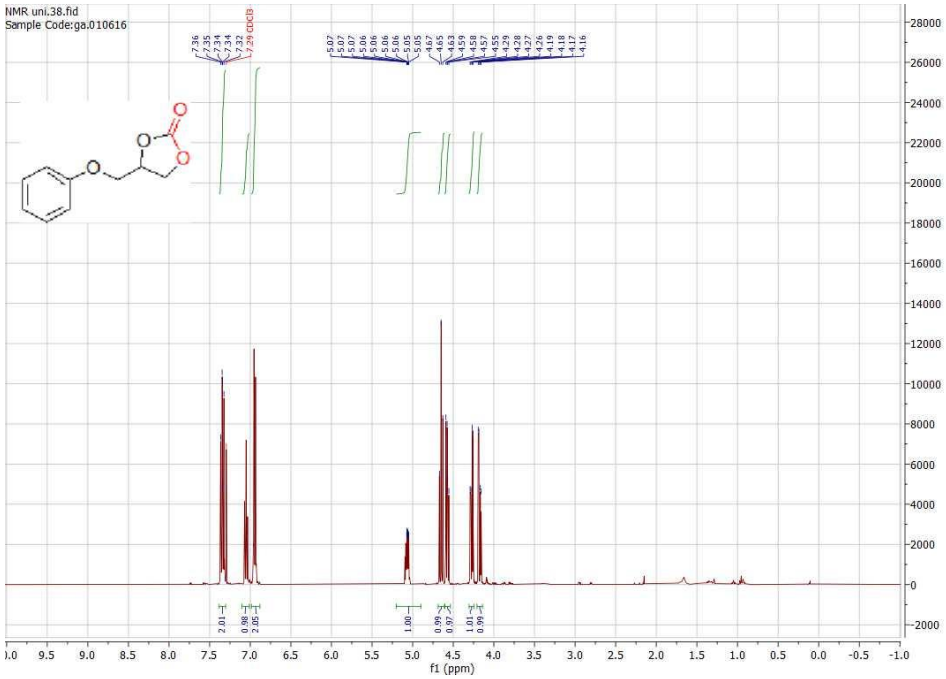

Figure S91. ^{1}H-NMR spectrum for (phenoxymethyl)ethylene carbonate in $CDCl_3$ as solvent

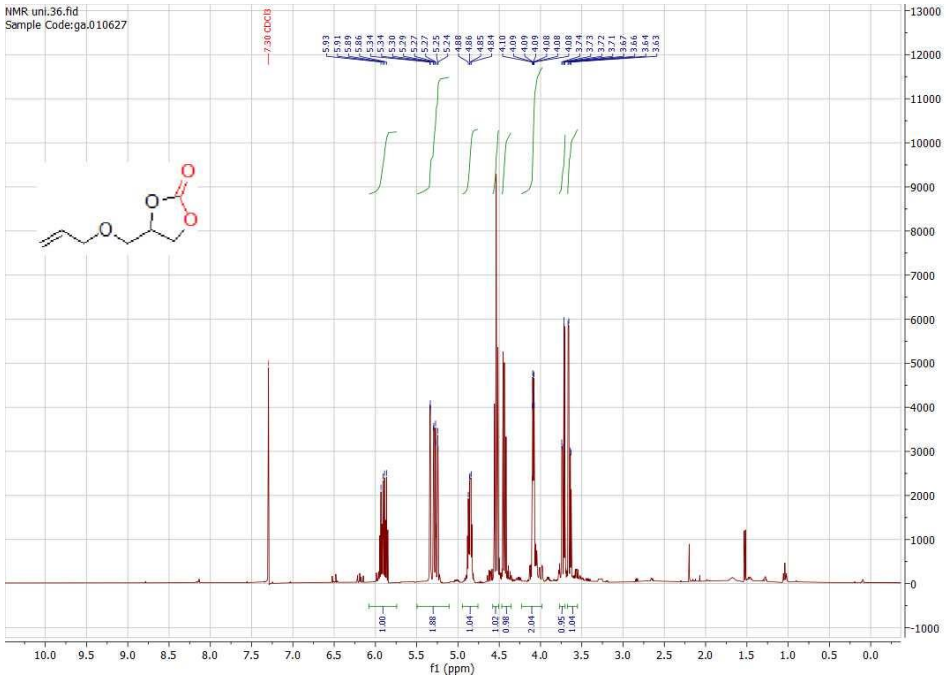

Figure S92. ^{1}H-NMR spectrum for allyl glycerol carbonate in $CDCl_3$ as solvent

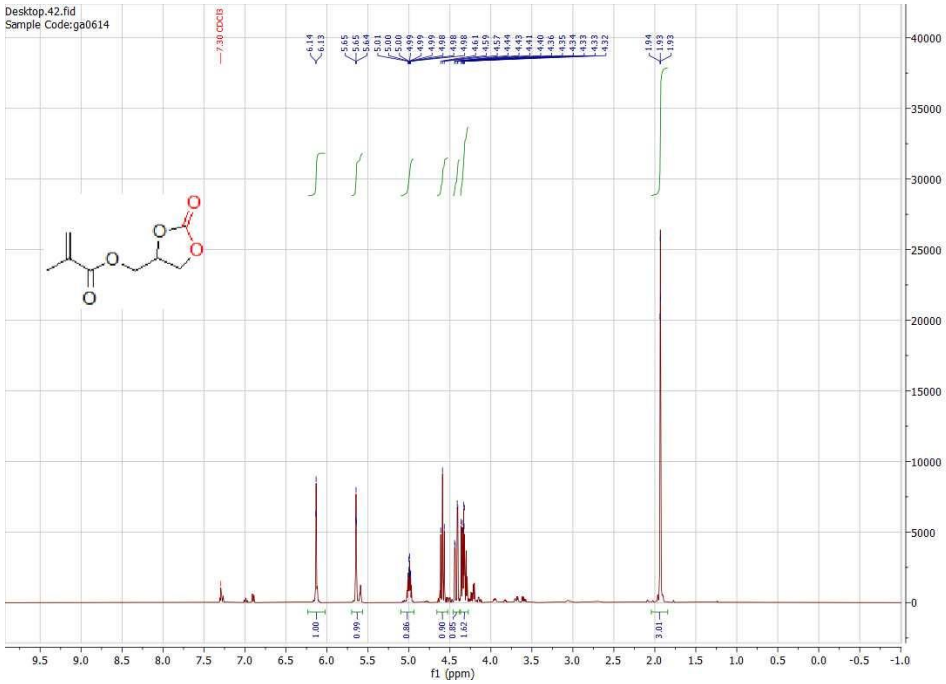

Figure S93. ^{1}H-NMR spectrum for (2-oxo-1,3-dioxolan-4-yl)-methyl methacrylate in $CDCl_3$ as solvent

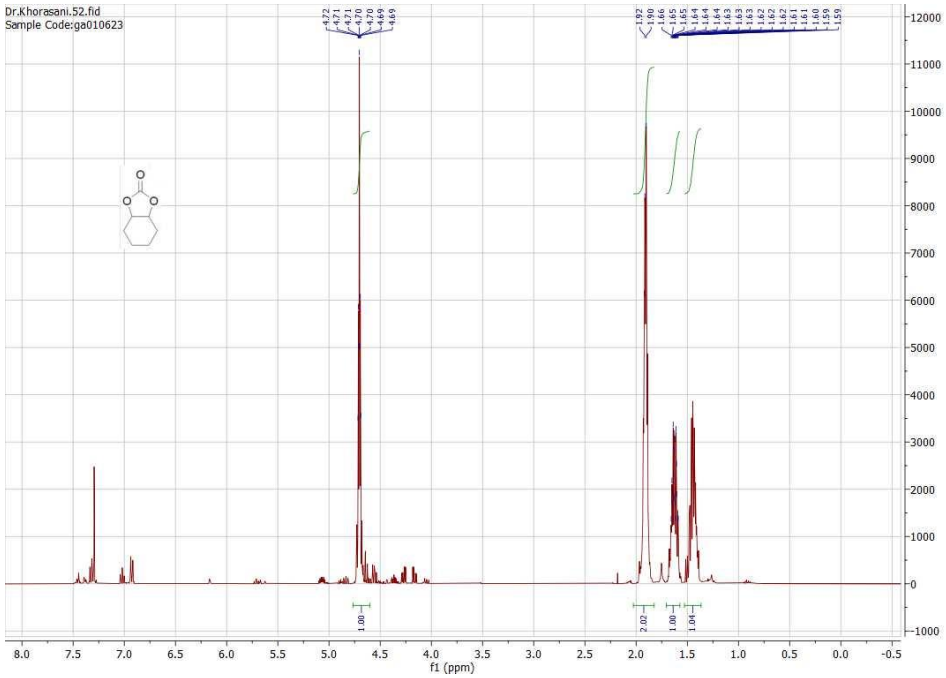

Figure S94. ^{1}H-NMR spectrum for cyclohexene carbonate in $CDCl_3$ as solvent

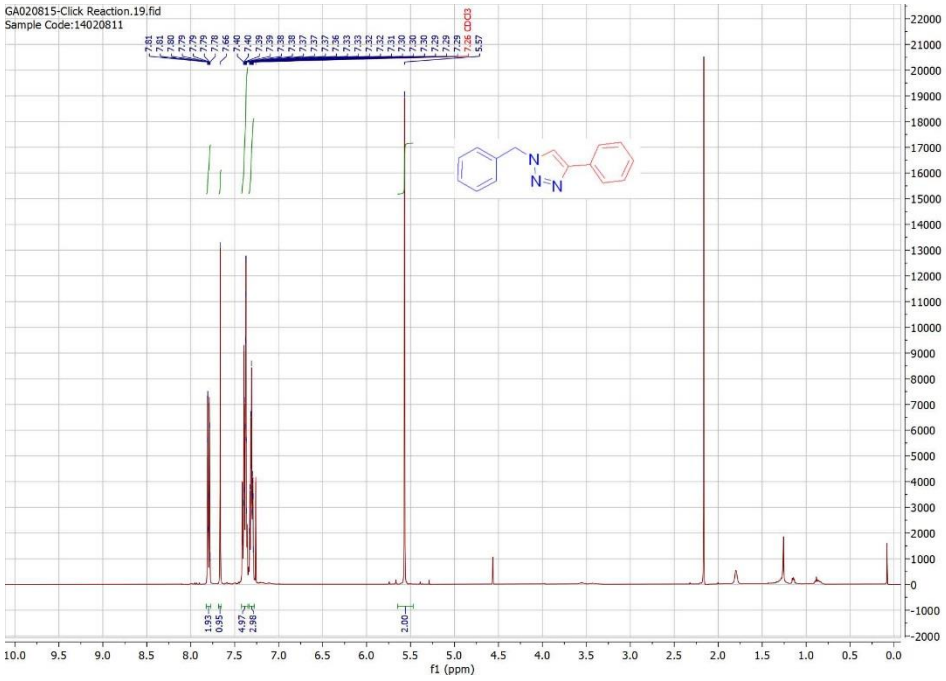

Figure S95. ^{1}H-NMR spectrum for 1-benzyl-4-phenyl-1H-1,2,3-triazole in $CDCl_3$ as solvent